Eur. Phys. J. B **11**, 101–119 (1999)

THE EUROPEAN PHYSICAL JOURNAL B

EDP Sciences

Polymer depletion interaction between a particle and a wall

A. Bringer[1], E. Eisenriegler[1,a], F. Schlesener[2], and A. Hanke[2]

[1] Institut für Festkörperforschung, Forschungszentrum Jülich, 52425 Jülich, Germany
[2] Fachbereich Physik, Bergische Universität Wuppertal, 42097 Wuppertal, Germany

Received 11 December 1998

Abstract. The attractive depletion interaction between a spherical particle and a planar wall in a dilute solution of long flexible nonadsorbing free polymer chains is found to depend crucially on the particle to polymer size ratio ρ. While the polymer-induced force between particle and wall decreases *monotonically* with increasing distance for large ρ, for small ρ it has a *maximum* at a distance of the order of the polymer size. For ideal chains we study the crossover from large to small ρ behavior in full quantitative detail. Besides the free energy of interaction and the force, we also discuss the spatial variations of the densities of chain-ends and chain-monomers near the wall and particle. Two independent procedures, (1) solving directly the diffusion equation for the density of ends in terms of planar and spherical waves and (2) minimizing the Ginzburg-Landau functional of the "magnetic analog" of the polymer problem, are used to obtain results *numerically* for a broad range of ratios of the three lengths particle size, polymer size and distance of particle from the wall. Besides previously known cases, we find two more interesting limiting regions of the length ratios for which *analytical* results can be obtained.

PACS. 05.70.Jk Critical point phenomena – 61.25.Hq Macromolecular and polymer solutions – 82.70.Dd Colloids

1 Introduction

A fundamental interaction in colloid physics is the depletion interaction between colloidal particles in a solution of free (non-adsorbing and non-grafted) polymer chains [1,2]. The interaction successfully explains phase diagrams of colloid-polymer mixtures [3–7]. Recent experimental techniques are even capable of measuring the force on a *single* colloidal particle [8–10].

Consider dilute polymer solutions where the overlap between different chains can be neglected. In most of the theoretical work on the depletion interaction the *p*olymers are treated as non-deformable *h*ard *s*pheres. This "phs"-approximation was introduced by Asakura and Oosawa [11] more than forty years ago. A long polymer chain is actually a *flexible* object and, in general, cannot be reduced to a single degree of freedom. Flexible chains interacting with colloidal particles have been investigated by means of integral equation techniques [12–14], Monte Carlo simulations [15,16], and scaling and field theories [17,18]. Analytical mean-field and scaling approaches have been considered also for the case of semidilute solutions of strongly overlapping flexible chains [17,19,20].

In this paper we investigate in detail the depletion interaction in a dilute and monodisperse solution of free flexible polymer chains and examine the range of validity of the phs-approximation of Asakura and Oosawa [11]. This is an important issue since the interpretation of experiments and the calculation of phase diagrams have been based mainly on this approximation.

We focus on the depletion interaction between a spherical particle and a planar wall, as in Figure 1. We denote the particle radius by R, the distance between the wall and the center of the particle by $D + R$, and the mean square end-to-end distance of the unperturbed chain by $d\mathcal{R}_x^2$, with d the dimension of space. For entropic reasons nonadsorbing chains avoid the space between the wall and particle, leading to an effective interaction which pushes the particle *towards* the wall [1–9,11].We find that the depletion interaction depends crucially on the particle to polymer size ratio $\rho = R/\mathcal{R}_x$. While the predictions of the phs-approximation are reasonable in the case of large ρ, they are qualitatively wrong if ρ is small. This is easy to understand in the limit $\rho = 0$ of a point particle. For the non-deformable polymer of the phs-model a point is a serious obstacle, but not for a flexible polymer, which can coil around it.

The behavior of flexible polymer chains is dominated by entropy and characterized by detail-independence ("universality") and scaling [21–23]. The simplest example is provided by random walks in an unbounded space with a large number of steps so that $\mathcal{R}_x$ is much larger

[a] e-mail: e.eisenriegler@fz-juelich.de

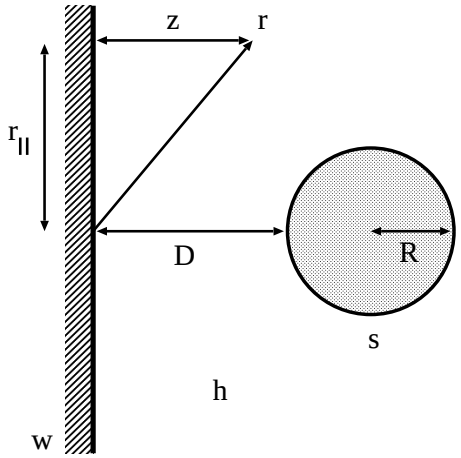

Fig. 1. A spherical particle s embedded in a polymer solution near a planar wall w. The monomer or end densities of polymer chains (not shown) depend on the position $\mathbf{r} = (\mathbf{r}_\parallel, z)$. We denote the surfaces of both s and w by σ and the space available for the polymers, *i.e.* the half space h to the right of w with the exception of the space occupied by the particle s, by h\s. For the ratios of the three lengths R, D, and the polymer extension $\mathcal{R}_x$ we frequently use the notations $D/\mathcal{R}_x = \vartheta$, $R/\mathcal{R}_x = \rho$, $D/R = \delta$.

than the length of one step. In this case the probability distribution for the mesoscopic end-to-end distance r only depends on the two lengths r and $\mathcal{R}_x$ *via* the ratio $r/\mathcal{R}_x$ (scaling). Thanks to the central limit theorem it has the same Gaussian form, both for walks in an isotropic continuum and walks on a cubic lattice (universality). Generally the behavior is very similar to the behavior of a system near a critical point, with $\mathcal{R}_x$ corresponding to the correlation length. The two types of systems can be related quantitatively by means of the so-called polymer-magnet analogy [21–23], compare also Appendix A. The fundamental properties of universality and scaling also hold for critical systems with surfaces [24,25] and can be applied to the physics of polymers in the presence of boundaries [26,27]. One can use the same powerful methods that have been developed in the areas of critical phenomena and field theory. These turn out to be very useful for our evaluation of the quantities of interest in the depletion-problem of Figure 1.

The depletion interaction in the case of Figure 1 has a universal form when the three lengths R, D, $\mathcal{R}_x$ are much larger than microscopic lengths and the persistence length characterizing the degree of stiffness of the chain. Since the free energy of polymer-induced interaction (or potential of mean force) δF is proportional to the number density n_b of chains in the bulk and is independent of the microscopic lengths, it has the scaling form

$$\delta F = p\, R^d\, Y(D/\mathcal{R}_x, R/\mathcal{R}_x) \qquad (1.1)$$

with $p = n_\mathrm{b} k_\mathrm{B} T$ the bulk osmotic pressure of the chains and Y a universal function. Because of the depletion *attraction*, Y is expected to be negative, to increase monotonically with $D/\mathcal{R}_x$, and to approach zero for $D/\mathcal{R}_x \to \infty$.

We find that the interaction described by the function Y has a rich structure. Our main focus is the simple case of *ideal* chains, in which the excluded volume interaction between monomers is neglected and which is widely used as a benchmark in the field [15]. For ideal chains we obtain the entire scaling function Y for *arbitrary* ratios $D/\mathcal{R}_x$ and $R/\mathcal{R}_x$. The crossover between the qualitatively different forms valid for large and small particle to polymer size ratios is exhibited in full detail.

The paper is organised as follows: In Section 2 we discuss a variety of interesting limiting cases of the free energy in (1.1), both for chains with and without interactions between monomers. In Section 3 we relate the free energy δF to the densities of chain-ends and chain-monomers. These two sections set the stage for our evaluation of the densities, δF, and the mean force for arbitrary length ratios in Sections 4 and 5 by means of two different approaches. The first is based on the well-known diffusion equation satisfied by the partition function of a random walk [21]. The partition function, or more precisely its Laplace transform with respect to the length of the walk, can be also obtained by minimizing a Ginzburg-Landau functional. This is the basis of the second approach. Our results are summarized in Section 6. The derivation of some of the results requires a background in field theory, even for the case of ideal chains. Technical details that can be skipped in a first reading are relegated to Appendices A-E.

2 Limiting forms of the interaction

A first impression of the rich behavior of the depletion interaction in equation (1.1) can be obtained by studying important limiting cases. We start by quoting a number of known results which apply to both chains with and without excluded volume interaction between monomers.

(i) For *large* particle radius R, one may use the Derjaguin-approximation replacing the interaction between the wall and the sphere by an interaction between the wall and a plate oriented parallel to the wall [28]. This leads to

$$\delta F \to p\, R^{\frac{d-1}{2}}\, \mathcal{R}_x^{\frac{d+1}{2}}\, Y_1(D/\mathcal{R}_x) \text{ for } D, \mathcal{R}_x \ll R \qquad (2.1)$$

with a scaling function Y_1, see [29] and Appendix B. As in the wall-plate problem the free energy in equation (2.1) leads to a polymer-induced force $\partial\, \delta F/\partial D$ pushing the spherical particle towards the wall which *decreases monotonically* with increasing D. A behavior with the form of (2.1) is also found in the phs-model of Asakura and Oosawa [11]. This is in line with the general expectation [4,6–9,15] that the phs-approximation works best for $\mathcal{R}_x \ll R$. Still it is not exact, even in this limit. For ideal chains in $d = 3$, for example, in the case $D = 0$ in which the spherical particle touches the wall, the phs-approximation for $\mid \delta F \mid$ is about 10% too small [29], compare the discussion near equation (4.13) and Figure 7 below.

(ii) For *small* particle radius one finds [18,30]

$$\delta F \to pR^{d-\frac{1}{\nu}}\,\mathcal{R}_x^{\frac{1}{\nu}}\,Y_2(D/\mathcal{R}_x) \text{ for } R \ll D, \mathcal{R}_x \qquad (2.2a)$$

with the scaling function

$$Y_2(D/\mathcal{R}_x) = A\,[\,M_{\rm h}(D/\mathcal{R}_x) - 1\,]\,. \qquad (2.2b)$$

Here ν is the Flory exponent [21–23], and A is a known positive universal number. The quantity $M_{\rm h}$ is the monomer density at distance D from the wall if the particle is absent (h stands for half space). It is normalized so that $M_{\rm h} \to 1$ for $D \to \infty$. Equation (2.2) only applies if the exponent $d - 1/\nu$ of R is positive encompassing both ideal polymers in $d > 2$ and self-repelling polymers in $d > 1$. For ideal polymers in $d > 2$, A is given [18] by $A_{\rm id} = 2\pi^{d/2}/\Gamma\left(\frac{d}{2} - 1\right)$. In the presence of excluded volume repulsion between monomers the value of A has been obtained in reference [27] for $d = 2$ and in reference [30] for $d = 3$. Note that the monomer density $M_{\rm h}$, which increases monotonically with D, has a point of inflection [21,26]. Thus the mean force $\partial\delta F/\partial D$ on the particle is not monotonic but has a *maximum* at a certain $D_{\max} \sim \mathcal{R}_x$. For $D < D_{\max}$ the attractive force *increases* with distance D.

The reason for the result (2.2) is that the N monomers j of the chain see the particle with center at $\mathbf{r}_{\rm s}$ as a point-like object if R is small. They feel a weak repulsive potential leading to a relative reduction $AR^{d-1/\nu}\,k\sum_j \delta(\mathbf{r}_{\rm s} - \mathbf{r}_j)$ of the Boltzmann weight, see equation (6.1) in reference [27]. The exponent $d - 1/\nu$ of R ensures the vanishing scaling dimension of this reduction. The constant $k = \mathcal{R}_x^{1/\nu}/N$ is independent of the length of the chain. In case of a semidilute solution of chains with excluded volume interaction between monomers we expect the same weight reduction (with the same amplitude A) as in the dilute case, provided $R \ll \mathcal{R}_x, \xi_E$. Here ξ_E is the Edwards screening length [21]. We mention another interesting consequence of this weight reduction: The free energy cost $F_{\rm bulk}$ of immersing the spherical particle in the bulk solution tends [18,27,30] for small radius R to $k_{\rm B}Tn_{\rm b}\mathcal{R}_x^{1/\nu}AR^{d-1/\nu}$. This expression is consistent with the result given in equation (5) of reference [17] in which ξ_E was denoted by ξ and determines the universal prefactor in this equation. Note that $n_{\rm b}\mathcal{R}_x^{1/\nu}$ is a convenient measure for the density of monomers and that $n_b\mathcal{R}_x^{1/\nu}\xi_E^{d-1/\nu}$ is a universal amplitude in the semidilute limit [22,23]. Similar "small sphere expansions" have been applied to mesoscopic particles in critical fluids [31–33].

(iii) Consider the free energy cost F of immersing the spherical particle in the dilute solution in the half space. This is related to δF by $\delta F = F - F_{\rm bulk}$. While $F_{\rm bulk}$ tends to $pAR^{d-1/\nu}\mathcal{R}_x^{1/\nu}$ for $R \ll \mathcal{R}_x$ and diverges for $\mathcal{R}_x \to \infty$, the quantity F remains finite and has the $\mathcal{R}_x$-independent behavior

$$F \to p\,R^d\,Y_3(D/R) \text{ for } R, D \ll \mathcal{R}_x. \qquad (2.3)$$

The reason is that in this regime the particle is immersed in a region which is already depleted due to the presence of the wall. For $R \ll D \ll \mathcal{R}_x$ equations (2.2) and (2.3) must both be satisfied. This requires

$$M_{\rm h}(D/\mathcal{R}_x) \to B(D/\mathcal{R}_x)^{1/\nu} \text{ for } D \ll \mathcal{R}_x \qquad (2.4)$$

with B a universal constant, and

$$Y_3(D/R) \to AB(D/R)^{1/\nu} \text{ for } R \ll D\,. \qquad (2.5)$$

Equations (2.2–2.5) imply

$$\partial\delta F/\partial D = \partial F/\partial D \to p\,(AB/\nu)R^{d-\frac{1}{\nu}}D^{\frac{1}{\nu}-1} \text{ for } R \ll D \ll \mathcal{R}_x\,. \qquad (2.6)$$

The force in (2.6) increases with increasing D since both A and B are positive [18,27,29,30], and $1/\nu$ is larger than 1 [21–23]. For ideal chains in three dimensions, $A = 2\pi$ and $B = 2$, see reference [27].

In cases (ii) and (iii) chain flexibility enters in a crucial way, and the phs-model is not even qualitatively correct. While the phs-model does yield a maximum in the D-dependence of the force if $R \ll D$, $\mathcal{R}_x$, it fails to describe the decrease of the interaction-strength with decreasing particle radius R and leads for $R \ll D \ll \mathcal{R}_x$ to the R-*independent* expression $\partial F^{(\rm phs)}/\partial D \sim p\,(\mathcal{R}_x D)^{(d-1)/2}$ for the force instead of the $\mathcal{R}_x$-independent expression (2.6) valid for flexible chains.

For the rest of this section we focus on the case of *ideal* chains in which simple explicit expressions can be obtained for the above limit functions Y_1, Y_2, Y_3. In this case we also find simple expressions in a region (iv) characterized by $\mathcal{R}_x \ll D$ with R arbitrary.

For ideal polymers in three dimensions the powers of the prefactors in equations (2.1) and (2.2a) are *identical* ($\nu = 1/2$ for ideal chains). Rewriting equation (1.1) as

$$\delta F = pR\,\mathcal{R}_x^2\,\mathcal{Y}(D/\mathcal{R}_x, R/\mathcal{R}_x) \qquad (2.7)$$

we see that the function of two variables $\mathcal{Y}(\vartheta, \rho)$ tends, both for $\rho \to \infty$ and $\rho \to 0$, to finite functions

$$\mathcal{Y}(\vartheta, \infty) = [Y_1(\vartheta)]_{\text{ideal},\, d=3} \qquad (2.8)$$

and

$$\mathcal{Y}(\vartheta, 0) = [Y_2(\vartheta)]_{\text{ideal},\, d=3}\,, \qquad (2.9)$$

respectively, of a single variable. Here $[Y_i]_{\text{ideal},\, d=3}$ with $i = 1$ and 2 denotes the functions Y_1 and Y_2 in equations (2.1–2.2) for ideal chains in $d = 3$. The two limit functions (2.8–2.9) are known explicitly [34]. Although their behavior for small ϑ

$$\mathcal{Y}(\vartheta, \infty) \to -4\pi\ln 2 + 4\sqrt{2\pi}\vartheta - \pi\vartheta^2, \quad \vartheta \to 0 \qquad (2.10)$$

and

$$\mathcal{Y}(\vartheta, 0) \to -2\pi + 4\pi\vartheta^2, \quad \vartheta \to 0 \qquad (2.11)$$

is quite different — leading to attractive mean forces $\sim \partial\mathcal{Y}/\partial\vartheta$ that decrease and increase with increasing ϑ, respectively — the two functions *merge* for large ϑ. In Appendix C we discuss the region of large ϑ with ρ *arbitrary* (called region (iv) above) and we show, in particular, that

$$\mathcal{Y}(\vartheta,\rho) \to -8\sqrt{2\pi}\vartheta^{-3}\exp[-\frac{1}{2}\vartheta^2], \quad \vartheta\to\infty\,, \qquad (2.12)$$

independent of ρ. The expression for large ϑ

$$[\mathcal{Y}(\vartheta,0)-\mathcal{Y}(\vartheta,\infty)]/|\mathcal{Y}(\vartheta,\rho)| \to \frac{1}{81}\exp[-4\vartheta^2],\ \vartheta\to\infty \qquad (2.13)$$

suggests that even the values $\mathcal{Y}(\vartheta=1,\rho)$ for different ρ's should be very close to one another. As shown below, our numerical investigations confirm this conjecture.

Now we turn to the limit function Y_3 in (2.3). For the case in which both R and D are small compared to the other mesoscopic lengths, the spherical particle can be viewed as a point defect located in the *wall* [35] with a defect strength $R^d A_{\rm snw}(D/R)$ that depends on the two small mesoscopic lengths R and D. Here the subscript snw stands for "sphere near wall". This case should be distinguished from the case of equation (2.2) in which only R is small and the spherical particle can be viewed as a point defect in the *bulk*. Note that the strengths of the wall-defect and the bulk-defect have length dimensions d and $d-\frac{1}{\nu}$, respectively. The explicit form of F in (2.3) follows from identifying $Y_3 = A_{\rm snw}$. This is discussed in Appendix D. There we also show how to calculate the function $A_{\rm snw}(D/R)$. For ideal polymers in $d=3$ one finds

$$[Y_3(D/R)]_{{\rm ideal},d=3} = 32\pi[\delta(\delta+2)]^{3/2} \times \sum_{\ell=0,1,2,\ldots}^{\infty} (\ell+\frac{1}{2})^2/[Q^{-2(\ell+\frac{1}{2})}-1] \qquad (2.14a)$$

with

$$\delta = D/R,\ Q = 1+\delta-[2\delta+\delta^2]^{1/2}\,. \qquad (2.14b)$$

For small and large δ this implies

$$[Y_3(\delta)]_{{\rm ideal},d=3} \to \begin{cases} 8\pi\{\zeta(3)+[\zeta(3)+\frac{1}{6}]\delta\}, & \delta\to 0 \\ 4\pi\delta^2 \end{cases}, \quad \delta\to\infty\,, \qquad (2.15)$$

with ζ the Riemann zeta function. Comparing (2.11) with the lower equation (2.15) confirms the consistency conditions (2.2b, 2.4, 2.5). The upper equation (2.15) and [18]

$$F_{\rm bulk} = pR\,\mathcal{R}_x^2(2\pi+4\sqrt{2\pi}\rho+\frac{4\pi}{3}\rho^2) \qquad (2.16)$$

yield

$$\mathcal{Y} \to -2\pi-4\sqrt{2\pi}\rho+8\pi[\zeta(3)-\frac{1}{6}]\rho^2+8\pi[\zeta(3)+\frac{1}{6}]\rho\vartheta \qquad (2.17)$$

to first order in ϑ for the scaling function $\mathcal{Y}(\vartheta,\rho)$ in (2.7) for small ρ. Equation (2.17) is, of course, consistent with the $\rho=0$ behavior of $\mathcal{Y}$ in equation (2.11).

Finally we note that the mean force onto a particle that *touches* the wall is given by

$$\left(\frac{\partial\,\delta F}{\partial D}\right)_{D=0} \to \begin{cases} pR\mathcal{R}_x 4\sqrt{2\pi}, & R\gg\mathcal{R}_x \\ pR^2\,8\pi[\zeta(3)+\frac{1}{6}], & R\ll\mathcal{R}_x \end{cases} \qquad (2.18)$$

as follows, respectively, from equation (2.10) and the upper equation (2.15) or (2.17). Likewise, the free energy of interaction $(\delta F)_{D=0}$ for large and small particles touching the wall follows from setting $\vartheta=0$ in equations (2.10, 2.17), respectively, and substituting into (2.7).

For later use we define the scaling function $f(\vartheta,\rho) = \partial\mathcal{Y}(\vartheta,\rho)/\partial\vartheta$ for the force in three dimensions by

$$\frac{\partial\,\delta F}{\partial D} = pR\mathcal{R}_x\, f(D/\mathcal{R}_x, R/\mathcal{R}_x)\,. \qquad (2.19)$$

3 Free energy of interaction and densities of chain-ends and chain-monomers

For a dilute solution of chains with or without excluded volume interactions between monomers the free energy δF and the mean force can be related to other observables, such as the bulk-normalized densities $\mathcal{E}(\mathbf{r})$ and $\mathcal{M}(\mathbf{r})$ of chain-ends and chain-monomers, respectively, in the presence of wall and particle. Here

$$\mathcal{E}(\mathbf{r})\to 1, \quad \mathcal{M}(\mathbf{r})\to 1 \qquad (3.1)$$

for $\mathbf{r}$ in the bulk, *i.e.* for $z\to\infty$, see Figure 1. Each of the two dimensionless quantities $\mathcal{E}$ and $\mathcal{M}$ is a function of the four ratios $r_\parallel/R$, z/R, D/R, and $\mathcal{R}_x/R$ of mesoscopic lengths. These functions are independent of most microscopic details. However, they are different for chains with and without excluded volume interactions.

The first of these relations is [18]

$$F = p\int_{\rm h} {\rm d}\mathbf{r}\,[\,\mathcal{E}_{\rm h}(z)-\mathcal{E}(\mathbf{r})\,] \qquad (3.2)$$

with $\mathcal{E}_{\rm h}$ the end density in the half space (h) without the spherical particle. The integral $\int_{\rm h}$ extends over the half space, with $\mathcal{E}(\mathbf{r})$ defined to be zero inside the particle. Equation (3.2) relates the free energy cost F of immersing the particle introduced above equation (2.3), to the depletion of the end density on immersing the particle. For $D\to\infty$ the quantity F tends to

$$F_{\rm bulk} = p\int {\rm d}\mathbf{r}\,[\,1-\mathcal{E}_{\rm s}(\mathbf{r})\,]\,, \qquad (3.3)$$

where $\mathcal{E}_{\rm s}$ is the end density around a spherical particle in the bulk without the wall.

The second relation is [27,29]

$$\partial F/\partial D \equiv \partial\delta F/\partial D = p\int {\rm d}\mathbf{r}_\parallel \left\{1-[\mathcal{M}(\mathbf{r})/\mathcal{M}_{\rm h}(z)]^{({\rm as})}\right\}\,, \qquad (3.4)$$

with $\mathcal{M}_{\rm h}(z) \equiv M_{\rm h}(z/\mathcal{R}_x)$ the monomer density in the half space introduced below equation (2.2b). Here (as) denotes the "asymptotic" scaling region close to the wall where $\mathcal{M}/\mathcal{M}_{\rm h}$ becomes independent of z [29] and depends only on $r_\parallel$, compare Figure 1. Equation (3.4) relates the force onto the particle, *i.e.* the reduction in the force onto the wall on immersing the particle, to the (relative) depletion of the monomer density close to the wall on immersing the particle and reflects a local density-force relationship [36].

To understand the increase of the force with increasing D mentioned below equation (2.2), it is useful to evaluate the integrand in equation (3.4). For ideal chains in $d > 2$ with $R \ll D$ and $D, r_\parallel \ll \mathcal{R}_x$,

$$1 - [\mathcal{M}(\mathbf{r})/\mathcal{M}_{\rm h}(z)]^{\rm (as)} = 4(d-2)(R/D)^{d-2}/\left[\,1 + (r_\parallel/D)^2\,\right]^{d/2}. \quad (3.5)$$

Thus on increasing D, the amplitude of the $r_\parallel$-dependence (3.5) of the monomer depletion close to the wall decreases while the width increases. In performing the integration in equation (3.4), the effect from the width dominates, and one finds the expression $pA_{\rm id}4R^{d-2}D$ for the force, which is consistent [27] with equation (2.6).

Another interesting application of equation (3.4) is in the region of large $\vartheta \equiv D/\mathcal{R}_x$ considered in equation (2.12). For $\vartheta \gg 1$, R arbitrary, and ideal chains in $d = 3$, the integrand of (3.4) reads

$$1 - [\mathcal{M}(\mathbf{r})/\mathcal{M}_{\rm h}(z)]^{\rm (as)} = 4\sqrt{\frac{2}{\pi}}\frac{R\,(R+D)}{(r_{\rm sw})^2}\frac{\mathcal{R}_x}{r_{\rm sw}-R} \times \exp\left[-\frac{(r_{\rm sw}-R)^2}{2\mathcal{R}_x^2}\right], \quad (3.6a)$$

as we show in Appendix C. Here

$$r_{\rm sw} = \sqrt{(R+D)^2 + r_\parallel^2} \quad (3.6b)$$

is the distance of a point $\mathbf{r}_\parallel$ in the surface of the wall (w) from the center of the spherical particle (s), compare Figure 1. Although the monomer density in (3.6) has a quite complicated R-dependence, it leads *via* (3.4) to a force with a simple linear R dependence. As checked in Appendix C, this force is indeed given by equation (2.19), with a ρ–independent function f determined by $\mathcal{Y}$ in equation (2.12). In the special case $\mathcal{R}_x \ll D \ll R$ of a large particle radius R, equation (3.6) reduces to the simpler expression

$$1 - [\mathcal{M}(\mathbf{r})/\mathcal{M}_{\rm h}(z)]^{\rm (as)} = 4\sqrt{\frac{2}{\pi}}\frac{\mathcal{R}_x}{\widetilde{D}}\exp\left[-\frac{\widetilde{D}^2}{2\mathcal{R}_x^2}\right] \quad (3.7a)$$

resulting from the Derjaguin-approximation [28] where

$$\widetilde{D} = D + \frac{r_\parallel^2}{2R} \quad (3.7b)$$

is the local surface-to-surface distance.

Relations (3.2) and (3.4) are valid for arbitrary ratios of the three lengths D, R, $\mathcal{R}_x$ and can be used in an explicit calculation of δF and $\partial\delta F/\partial D$, respectively. First consider equation (3.2). The end density is related to the partition function $Z(\mathbf{r}, \mathbf{r}')$ of a polymer chain with ends fixed at $\mathbf{r}$ and $\mathbf{r}'$ by

$$\mathcal{E}(\mathbf{r}) = \int_{\rm h\backslash s} {\rm d}\mathbf{r}'\, Z(\mathbf{r}, \mathbf{r}') / \int {\rm d}\mathbf{r}'\, Z_{\rm bulk}(\mathbf{r}, \mathbf{r}')\,. \quad (3.8)$$

While the integration in the denominator extends over all space, the integration in the numerator is confined to the space h\s bounded by the wall and particle surfaces, see Figure 1. For an ideal chain the partition function obeys the diffusion equation for a heat kernel [18,21,23,26], where the role of the time is taken by the mean square end-to-end distance $\mathcal{R}_x^2$. To make the $\mathcal{R}_x$ dependence explicit, it is convenient to use the abbreviation

$$\mathcal{R}_x^2 = 2L\,. \quad (3.9)$$

For well separated micro- and mesoscopic lengths the repulsive surfaces σ of wall and particle can be simply taken into account by imposing Dirichlet boundary conditions for $Z(\mathbf{r}, \mathbf{r}') \equiv Z(L; \mathbf{r}, \mathbf{r}')$, *i.e.* by requiring

$$Z(L; \mathbf{r}, \mathbf{r}') \to 0 \quad (3.10)$$

for $\mathbf{r}$ or $\mathbf{r}'$ tending to the surfaces σ. Then $\mathcal{E}(\mathbf{r}) \equiv \mathcal{E}(L, \mathbf{r})$ is determined by the diffusion equation

$$\left(\frac{\partial}{\partial L} - \Delta_{\mathbf{r}}\right)\mathcal{E}(L, \mathbf{r}) = 0\,, \quad (3.11a)$$

with the "initial condition"

$$\mathcal{E}(L = 0, \mathbf{r}) = 1 \quad (3.11b)$$

for any interior point $\mathbf{r}$ of the bounded space h\s and the boundary condition

$$\mathcal{E}(L, \mathbf{r} \to \sigma) \to 0 \quad (3.11c)$$

for any $L > 0$ if $\mathbf{r}$ approaches the surfaces σ of either wall or particle.

In Section 4 we solve equation (3.11) for $\mathcal{E}$ with wave mechanical scattering methods (WSM) and calculate F from (3.2). In Section 5 we make use of the polymer-magnet analogy (PMA) [21–23,26,27] and calculate $\mathcal{M}(\mathbf{r})$ and $\partial F/\partial D$ from a function $\chi(\mathbf{r})$ that minimizes a Ginzburg-Landau functional. The accuracy of our results can be checked (i) by comparing $\partial F/\partial D$ with $\mathcal{M}$ by means of equation (3.4) and (ii) by comparing F from WSM with $\partial F/\partial D$ from PMA.

4 Density of chain ends from diffusion equation

Here we determine the normalized density $\mathcal{E}$ of chain ends in three dimensions from equation (3.11) by superposing eigenfunctions of the Laplacian $\Delta_{\mathbf{r}}$. Before considering the geometry of Figure 1 we illustrate the method for the simple geometries of free space, the half space, and a spherical particle in free space with normalized end-densities $\mathcal{E}_{\rm bulk}$, $\mathcal{E}_{\rm h}$, $\mathcal{E}_{\rm s}$, respectively.

4.1 Method of solution

The general solution $E(L;\mathbf{r})$ of the diffusion equation (3.11a)

$$\frac{\partial E}{\partial L} = \Delta_{\mathbf{r}} E \tag{4.1}$$

in *free space* is given by the Fourier integral $E = \int \mathrm{d}\mathbf{k}\; w(\mathbf{k}) \exp(\mathrm{i}\mathbf{k}\mathbf{r} - Lk^2)$. It contains an arbitrary weight function w, which is fixed by the initial condition. For example, to generate the normalized partition function of a free polymer with fixed ends at points zero and $\mathbf{r}$ (or free heat kernel) $E = \tilde{Z}_{\mathrm{bulk}}(L;\mathbf{r})$ with $\tilde{Z}_{\mathrm{bulk}}(0;\mathbf{r}) = \delta(\mathbf{r})$, the weight must be chosen $\mathbf{k}$-independent, $w = (2\pi)^{-3}$, implying $\tilde{Z}_{\mathrm{bulk}}(L;\mathbf{r}) = (4\pi L)^{-3/2} \exp(-r^2/(4L))$. Another example is the end density $E = \mathcal{E}_{\mathrm{bulk}} \equiv \int \mathrm{d}\mathbf{r} \tilde{Z}_{\mathrm{bulk}}$, which is unity in this case and can be generated by the weight $w = \delta(\mathbf{k})$.

In the presence of *geometrical restrictions* it is also possible to represent the general solution of the diffusion equation in the restricted space $\mathcal{V}$ by the integral

$$E = \int \mathrm{d}\mathbf{k}\; w(\mathbf{k}) B(\mathbf{k},\mathbf{r}) \mathrm{e}^{-Lk^2}. \tag{4.2}$$

The free space plane wave basis must be replaced by a complete set of solutions B of the boundary value problem

$$(\Delta_{\mathbf{r}} + k^2) B = 0 \quad \text{for } \mathbf{r} \text{ in } \mathcal{V} \tag{4.3a}$$

$$B(\mathbf{k},\mathbf{r}) = 0 \quad \text{for } \mathbf{r} \text{ on boundaries}. \tag{4.3b}$$

Furthermore the weight function w must be chosen to satisfy the initial condition (3.11b) for $E = \mathcal{E}_{\mathcal{V}}$

$$1 = \int \mathrm{d}\mathbf{k}\; w(\mathbf{k}) B(\mathbf{k},\mathbf{r}) \text{ for } \mathbf{r} \text{ in } \mathcal{V}. \tag{4.4}$$

For the two following examples, which are effectively one-dimensional with $\int \mathrm{d}\mathbf{k} = \int_0^\infty \mathrm{d}k$, the basis ($B$) and weight functions ($w$) are easily determined. In the half space $z > 0$, $\mathcal{E}_{\mathrm{h}}$ only depends on z. The basis-functions are $B(k,z) = \sin(kz)$, the weight is $w(k) = 2/(\pi k)$, and $E = \mathcal{E}_{\mathrm{h}} = (2/\pi) \int_0^\infty \mathrm{d}k\; k^{-1} \sin(kz)\; \mathrm{e}^{-Lk^2}$. For $L = 0$ and $z > 0$ this expression for $\mathcal{E}_{\mathrm{h}}$ equals 1. For $L > 0$ the integral may be evaluated yielding $\mathcal{E}_{\mathrm{h}} = \mathrm{erf}(z/(\sqrt{2}\mathcal{R}_x))$ in terms of the error function erf [37].

In the region $|\mathbf{r}| > R$ outside a spherical particle of radius R in free space, $E = \mathcal{E}_{\mathrm{s}}$ only depends on $r = |\mathbf{r}|$. The basis functions fulfilling the boundary condition on the sphere are in this case $B(k,r) = \sin(k[r-R])/r$. Integrating with the weight function $w(k) = 2R/(\pi k)$ generates the solution $(R/r)\; \mathrm{erf}\left([r-R]/(\sqrt{2}\mathcal{R}_x)\right)$. At $L = \mathcal{R}_x = 0$, this solution equals R/r, not 1 as required. To correct this, one must add the harmonic function $1 - R/r$, which obeys equation (4.1) and the boundary condition, *i.e.* it is a basis-function with $k = 0$. This leads to $\mathcal{E}_{\mathrm{s}} = 1 - (R/r)\; \mathrm{erfc}\left([r-R]/(\sqrt{2}\mathcal{R}_x)\right)$ [38,18] with erfc the error function complement [37].

For $L \to \infty$ only the $k = 0$ contribution survives, *i.e.*, $\mathcal{E}_{\mathrm{s}}(\infty,\mathbf{r}) = 1 - R/r$. As in equation (3.8), $\mathcal{E}_{\mathcal{V}}(\infty,\mathbf{r})$ represents the fraction of the number of configurations of a chain with one end fixed at $\mathbf{r}$ and infinite length which survive on introducing the geometrical restrictions leading to $\mathcal{V}$. This fraction is finite in case of the finite inaccessible region s of the sphere in three dimensional free space but vanishes in case of the half space $\mathcal{V}$=h in which the inaccessible region w is of infinite extent. Likewise, no $k = 0$ contribution arises, *i.e.* $\mathcal{E}(\infty,\mathbf{r})$ vanishes, for the case $\mathcal{V} = \mathrm{h}\backslash\mathrm{s}$ of Figure 1, compare equation (4.12) below.

We close this subsection by commenting on the monomer density $\mathcal{M}_s$ outside a spherical particle in free space. For $L \to \infty$ it tends to the square of $\mathcal{E}_s$, *i.e.* to $\mathcal{M}_{\mathrm{s}}(\infty,\mathbf{r}) = (1 - R/r)^2$, compare reference [18] and equation (5.8) below. This result not only applies to a solution of noninteracting ideal chains but has also been derived [20] for a semidilute solution by treating the excluded volume interaction between chains in mean-field fashion. Also in this case $\mathcal{M}_{\mathrm{s}}$ is the square of a harmonic function and has the form given above, provided the screening length ξ_E is much larger than R and r. In the presence of fluctuations we again expect the variation of $\mathcal{M}_{\mathrm{s}}$ with r in the domain $R, r \ll \mathcal{R}_x, \xi_E$ to be independent of $\mathcal{R}_x$ and ξ_E (and thus independent of the degree of overlap between the chains) and to only depend on the ratio r/R. However, this dependence is different from above and involves non-integer exponents such as $1/\nu$.

4.2 Particle in half-space

Now we turn to the geometry of Figure 1, where $\mathcal{V} = \mathrm{h}\backslash\mathrm{s}$ is of lower symmetry, and more computational effort is needed to construct the functions B and w. Each point $\mathbf{r} = (x,y,z)$ in h\s has the position vectors,

$$\mathbf{c} = (x, y, z - \mathcal{C}) = c\; (\cos\phi\; \sin\Theta, \sin\phi\; \sin\Theta, \cos\Theta)$$

and

$$\bar{\mathbf{c}} = (x, y, z + \mathcal{C}) = \bar{c}\; (\cos\phi\; \sin\bar{\Theta}, \sin\phi\; \sin\bar{\Theta}, \cos\bar{\Theta})\,,$$

with respect to the center of the spherical particle s and its mirror image $\bar{\mathrm{s}}$ with respect to the wall surface $z = 0$ (see Fig. 2). Here $\mathcal{C} = D + R$.

The first step, finding the basis functions B from equation (4.3a) with equation (4.3b) specified as $B(\mathbf{k},[x,y,0]) = B(\mathbf{k},[\, R\, \cos\phi\, \sin\Theta,\; R\, \sin\phi\, \sin\Theta,\; \mathcal{C} + R\, \cos\Theta]) = 0$, is equivalent to *wave-mechanical scattering by hard walls*. The B's may be expressed as a superposition of the combination $\mathrm{e}^{\mathrm{i}\mathbf{k}\mathbf{r}} - \mathrm{e}^{\mathrm{i}\bar{\mathbf{k}}\mathbf{r}}$ of two plane waves with wave vectors $\mathbf{k} = (\; p\; \cos\alpha,\; p\; \sin\alpha,\; q\;)$ and $\bar{\mathbf{k}} = (\; p\; \cos\alpha,\; p\; \sin\alpha,\; -q\;)$, respectively, where $k^2 = p^2 + q^2$ and $q \geq 0$, and of the two combinations

$$J_{\Lambda,M} = j_\Lambda(kc) Y_{\Lambda,M}(\Theta,\phi) - (-1)^{\Lambda-M} j_\Lambda(k\bar{c}) Y_{\Lambda,M}(\bar{\Theta},\phi), \tag{4.5a}$$

$$N_{\Lambda,M} = n_\Lambda(kc) Y_{\Lambda,M}(\Theta,\phi) - (-1)^{\Lambda-M} n_\Lambda(k\bar{c}) Y_{\Lambda,M}(\bar{\Theta},\phi) \tag{4.5b}$$

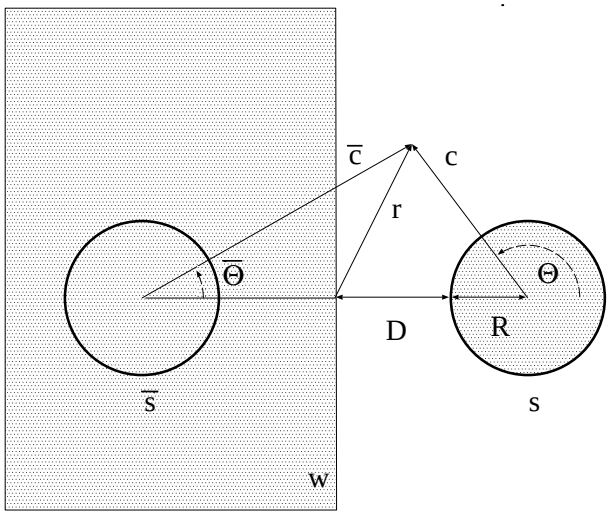

Fig. 2. Distance vectors $\mathbf{c}$, $\bar{\mathbf{c}}$ from the centers of the spherical particle s and its mirror image $\bar{\text{s}}$.

of spherical waves scattered from the spherical particle s and its mirror image $\bar{\text{s}}$. The radial dependence is given by spherical Bessel- and Neumann-functions, j_Λ and n_Λ, and the angular dependence by spherical harmonics $Y_{\Lambda,M}$ [37]. Each of the three combinations satisfies equation (4.3a) and vanishes in the surface $z = 0$ of the wall. For $E = \mathcal{E}$ there is still cylindrical symmetry, and only solutions independent of the azimuthal angle ϕ are of interest, which follow from averaging the plane waves with respect to the azimuthal angle α of the wave vector and considering only spherical waves with $M = 0$. Thus the basis functions have the form

$$B(\mathbf{k},\mathbf{r}) = B(k,q,\mathbf{r}) = \frac{1}{2\pi\mathrm{i}}\int_{-\pi}^{\pi} \mathrm{d}\alpha (e^{\mathrm{i}\mathbf{kr}} - e^{\mathrm{i}\bar{\mathbf{k}}\mathbf{r}}) + \sum_{\Lambda} \Gamma_\Lambda (J_{\Lambda,0} + \mathrm{i}N_{\Lambda,0})\,. \quad (4.6)$$

In the sum over spherical waves in (4.6) we have chosen the combination which contains only outgoing waves for $r \to \infty$ (a convenient way to generate an *orthonormal continuum* basis B). The coefficients, $\boldsymbol{\Gamma} = (\Gamma_\Lambda\colon\ \Lambda = 0,1,2,...)$ are determined by the boundary condition (4.3b) on the surface of the spherical particle s.

All contributions to B in equation (4.6) may be expanded in series of spherical harmonics $Y_{l,0}(\Theta,\phi)$ around the center of the spherical particle s. It is convenient to use Legendre-polynomials $P_l(\cos\Theta) = \sqrt{(2l+1)/(4\pi)}Y_{l,0}(\Theta,\phi)$ instead of $Y_{l,0}$. The plane wave part is

$$\frac{1}{2\pi\mathrm{i}} \int_{-\pi}^{\pi} \mathrm{d}\alpha (\mathrm{e}^{\mathrm{i}\mathbf{kr}} - \mathrm{e}^{\mathrm{i}\bar{\mathbf{k}}\mathbf{r}}) = \sin(qz)\ J_0(pc\sin\Theta) = \sum_l P_l(\cos\Theta)\ a_l\ P_l(\cos\beta)\, j_l(kc).$$

Here $J_0(\zeta) = \int_{-\pi}^{\pi} \mathrm{d}\alpha \exp(\mathrm{i}\zeta\cos\alpha)/(2\pi)$ is the cylinder function of order zero, β is the polar angle of the wave vector defined by $\cos\beta = q/k$, and $a_l = (2l+1)(-1)^{l/2}\sin(q\mathcal{C})$ for l even, $(2l+1)(-1)^{(l-1)/2}\cos(q\mathcal{C})$ for l odd. The corresponding expansions for the combinations of spherical waves are

$$J_{\Lambda,0} = \sum_l P_l(\cos\Theta)\mathcal{M}^{(j)}_{\Lambda,l},\ N_{\Lambda,0} = \sum_l P_l(\cos\Theta)\mathcal{M}^{(n)}_{\Lambda,l}\ , \quad (4.7)$$

with $\mathcal{M}^{(j)}_{\Lambda,l} = \left(\delta_{\Lambda,l} - m^{(j)}_{\Lambda,l}(k\mathcal{C})\right) j_l(kc)$ and $\mathcal{M}^{(n)}_{\Lambda,l} = \delta_{\Lambda,l}\ n_l(kc) - m^{(n)}_{\Lambda,l}(k\mathcal{C})\ j_l(kc)$. Here the matrix elements $m^{(j)}_{\Lambda,l}$ and $m^{(n)}_{\Lambda,l}$ follow from equation (4.5) by expressing the waves $j_\Lambda P_\Lambda$ and $n_\Lambda P_\Lambda$ scattered from $\bar{\text{s}}$ in terms of those scattered from s by using for $\Lambda = 0$

$$f_0(k\bar{c}) = \sum_{l=0}^{\infty}(2l+1) f_l(2k\mathcal{C}) j_l(kc) P_l(-\cos\Theta)\,,$$

and for $\Lambda = 1,2,...$ the recursion relation

$$f_{l+1}(k\bar{c})P_{l+1}(\cos\bar{\Theta}) = \frac{l}{l+1} f_{l-1}(k\bar{c})P_{l-1}(\cos\bar{\Theta}) - \frac{2l+1}{2k(l+1)}\frac{\partial}{\partial\mathcal{C}}\left[f_l(k\bar{c})P_l(\cos\bar{\Theta})\right]$$

for the Bessel- and Neumann-functions $f = j$ or n. The derivative in the last relation is at fixed c and Θ (*cf.* Fig. 2). The boundary condition on the surface of the spherical particle s implies the linear equations

$$\left(\mathcal{M}^{(j)} + \mathrm{i}\mathcal{M}^{(n)}\right)_{c=R} \boldsymbol{\Gamma} = -\mathbf{A} \quad (4.8)$$

with $\mathbf{A} = [a_l\, P_l(\cos\beta)\, j_l(kR)\colon\ l = 0,1,2,...]$. Inserting the solution $\boldsymbol{\Gamma} = \boldsymbol{\Gamma}(k\mathcal{C}, kR, \cos\beta)$ of (4.8) into equation (4.6) completely determines the basis functions B.

It is important to notice that this construction gives a complete orthonormal basis for cylindrically symmetric functions in the sense

$$\int_{\mathrm{h}\backslash\mathrm{s}} \mathrm{d}\mathbf{r}\, B^\star(\mathbf{k},\mathbf{r})B(\mathbf{k}',\mathbf{r}) = (2\pi)^3\,\delta(\mathbf{k}-\mathbf{k}')$$
$$\int_{q>0} \mathrm{d}\mathbf{k}\, B^\star(\mathbf{k},\mathbf{r}')B(\mathbf{k},\mathbf{r}) = (2\pi)^3\,\delta(\mathbf{r}'-\mathbf{r}). \quad (4.9)$$

The second step, determination of the weight function

$$w(\mathbf{k}) = \frac{1}{(2\pi)^3}\int \mathrm{d}\mathbf{r}\, B^\star(\mathbf{k},\mathbf{r})$$

from equation (4.4), is then straightforward. Using equation (4.3a) for B and Gauss' theorem, we express w as an integral over the boundary of h\s [39]

$$w(\mathbf{k}) = -\frac{1}{(2\pi)^3 k^2}\oint \mathrm{d}\mathbf{S}(\mathbf{r})\cdot\nabla B^\star(\mathbf{k},\mathbf{r}), \quad (4.10)$$

with $\mathrm{d}\mathbf{S}$ the vectorial surface element pointing away from h\s. Since the integral over the surface of the hemisphere

at infinite distance ($r \to \infty$ with $z > 0$) vanishes, $w = w_1 + w_2$ consists of the integrals

$$w_1(\mathbf{k}) = \frac{1}{(2\pi)^2 k^2} \int_0^\infty \mathrm{d}r_\parallel \, r_\parallel \, \frac{\partial}{\partial z} B^\star(\mathbf{k}, \mathbf{r}) \Big|_{z=0} ,$$

$$w_2(\mathbf{k}) = \frac{R^2}{(2\pi)^3 k^2} \int \mathrm{d}\Omega \, \frac{\partial}{\partial c} B^\star(\mathbf{k}, \mathbf{r}) \Big|_{c=R} ,$$

over the wall surface $z = 0$ and over the surface of the spherical particle s, respectively. In the second integral only the first spherical harmonic $P_0(\cos\Theta)$ contributes. By using the first vector-component of equation (4.8) one obtains

$$w_2(\mathbf{k}) = \frac{2R\,\mathrm{i}\,\Gamma_0}{\pi^2 k^2 \, \sin(kR)} \quad .$$

In the first integral w_1 the plane waves of equation (4.6) lead to a singular contribution $\propto \delta(1 - \cos\beta)$ which projects $\mathbf{k}$ onto the z-direction, while the spherical waves of equation (4.6) lead to regular contributions. The latter contain the integrals

$$I_\Lambda^{(f)} = \frac{\partial}{\partial(k\mathcal{C})} \left[\int_{k\mathcal{C}}^\infty \mathrm{d}c' \; c' \; f_\Lambda(c') \; P_\Lambda \left(\frac{k\mathcal{C}}{c'} \right) \right]$$

where $f = j$ or n, with the result $I_\Lambda^{(j)} = -(-1)^{\Lambda/2} \sin(k\mathcal{C})$ for Λ even, $(-1)^{(\Lambda-1)/2} \cos(k\mathcal{C})$ for Λ odd, and $I_\Lambda^{(n)} = (-1)^{\Lambda+1} I_{\Lambda+1}^{(j)}$. This leads to

$$w(\mathbf{k}) = \frac{1}{\pi^2 k^3} \left(\delta(1 - \cos\beta) + 2 \sum_\Lambda \Gamma_\Lambda (I_\Lambda^{(j)} + \mathrm{i} I_\Lambda^{(n)}) + \frac{2kR\,\mathrm{i}\,\Gamma_0}{\sin(kR)} \right) . \quad (4.11)$$

From w and the basis functions B in (4.6) the solution of the diffusion equation, $E = \mathcal{E}$, follows directly from the integral representation (4.2). It can be simplified by evaluating the $\mathbf{k}$-integration with spherical coordinates. All the terms in equations (4.6, 4.11) depend on k and $b = \cos\beta = q/k$. The integration over b may be done first. It is convenient to introduce $\mathbf{e}_z = [0, 0, 1]$ and $\tilde{B}(k, \mathbf{r}) = \int_0^1 \mathrm{d}b \; w_r(\mathbf{k}) \, B(\mathbf{k}, \mathbf{r})$, where w_r collects the regular parts of w in equation (4.11). The end density $\mathcal{E}$ for the geometry of Figure 1 is then obtained as

$$\mathcal{E}(L, \mathbf{r}) = \frac{2}{\pi} \int_0^\infty \frac{\mathrm{d}k}{k} \left[B(k\mathbf{e}_z, \mathbf{r}) + \tilde{B}(k, \mathbf{r}) \right] \mathrm{e}^{-Lk^2} . \quad (4.12)$$

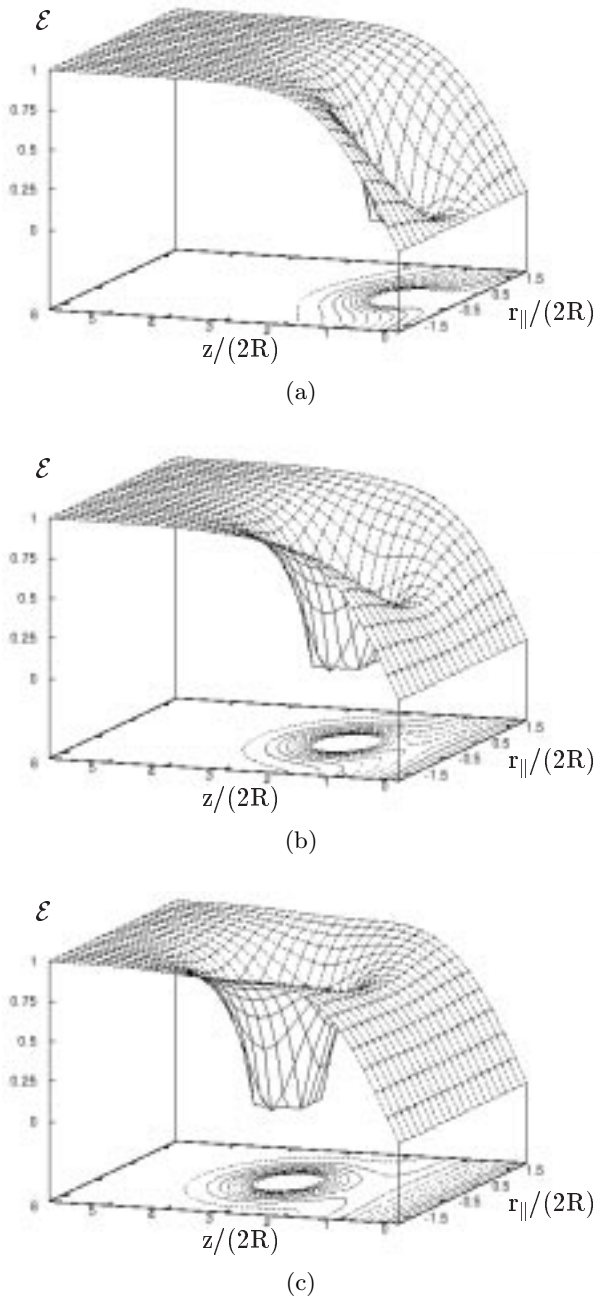

Fig. 3. Normalized density of chain-ends $\mathcal{E}(r_\parallel, z)$ for $R/\mathcal{R}_x = 1/4$ and $D/R = 1$ (a), 3 (b), 5 (c). The deviation $|\mathcal{E} - \mathcal{E}_\mathrm{h}|$ from the density $\mathcal{E}_\mathrm{h}$ without the sphere decreases if the sphere approaches the wall.

4.3 Numerical procedures and special results

The crucial step in the explicit evaluation of $\mathcal{E}$ is the calculation of the vector of coefficients $\boldsymbol{\Gamma}$, which is carried out numerically from equation (4.8). The l-expansions (4.7) for $J_{\Lambda,0}$ and $N_{\Lambda,0}$, converge rapidly for l larger than the arguments of the Bessel functions (k times the geometrical dimensions R, D, and r). The infinite set of linear equations can always be truncated at a proper l. A convenient cutoff (in the sense of not too much numerical effort) is $l_\mathrm{c} \cong 10$. Due to the Gaussian weight in equation (4.12) only $k < \mathcal{O}(1/\mathcal{R}_x)$ is needed, and this cutoff then covers the range $0 < R, D \leq 7\mathcal{R}_x$. The Gaussian weight eliminates large k contributions for which the truncated B-functions do not fulfill the boundary conditions on the sphere.

The influence of boundaries on the end-density distribution $\mathcal{E}$ vanishes exponentially when the distance from the boundary becomes large compared to $\mathcal{R}_x$. This can be seen explicitly for the two cases, single wall and single sphere in infinite space, from the analytic formulas given in subsection 4.1. It is also true when several objects, *e.g.* wall and sphere are present simultaneously. The important new phenomenon is the *interference* of the zones of reduced density, *i.e.* of the depletion layers, if the distance D between the objects is of the order of $\mathcal{R}_x$ or smaller. This effect is illustrated in the sequence of plots in Figure 3, where $\mathcal{E}$ is shown for $R = \mathcal{R}_x/4$ and $D/R = 1, 3, 5$. The density $\mathcal{E} = \mathcal{E}(r_\parallel, z)$ is plotted as a surface over the $(r_\parallel, z)$ plane. The depletion layers merge for the smallest D (Fig. 3a) in the sense that the polymers do not penetrate the space between wall and sphere. They are almost completely separated for the largest D (Fig. 3c). When the sphere approaches the wall the size of $\mathcal{E}_\mathrm{h} - \mathcal{E}$ is reduced. The corresponding reduction of F in equation (3.2) implies the depletion attraction between the sphere and the wall.

4.4 Free energy and force

For large D and various ratios $\rho \equiv R/\mathcal{R}_x$, we have checked that our procedure for calculating F quantitatively reproduces the form (2.16) of F_bulk. For general D our approach necessarily leads to the scaling structure of the free energy $\delta F = F - F_\mathrm{bulk}$, as given in equation (2.7). Figure 4a shows our results for the dependence of the scaling function $\mathcal{Y}$ in equation (2.7) on the scaled distance $\vartheta \equiv D/\mathcal{R}_x$ for various values of the particle to polymer size ratio ρ. Corresponding plots for the scaling function $f = \partial\mathcal{Y}/\partial\vartheta$ of the force in equation (2.19) are shown in Figure 4b.

Two features of Figures 4a and 4b are apparent: (a) For particle to polymer size ratio ρ smaller than $\rho_\mathrm{c} \approx 0.7$, the force passes through a *maximum* (and the free energy through a point of inflection) as the distance D increases. (b) For not too small reduced distances ϑ the scaling functions $\mathcal{Y}$ and f are independent of ρ. It is remarkable that the ρ-independence not only applies for large values of ϑ where equations (2.12, 2.13) hold, but also persists down to ϑ-values of order 1. Compare the discussion below equation (2.13).

Both the positions $\vartheta = \vartheta_\mathrm{max}(\rho)$ and the heights $f(\vartheta_\mathrm{max}(\rho), \rho)$ of the maxima in Figure 4b depend upon the size ratio ρ, as indicated by the curves with full dots in Figures 5a and 5b, respectively. The curve with empty dots in Figure 5b shows the ρ-dependence of $f(0, \rho)$ for a spherical particle that *touches* the wall. Information on the free energy for this latter case is contained in Figure 6, where $F/(pR^3)\big|_{D=0}$ is plotted *versus* ρ in the range $0 < \rho < 1$ (Fig. 6a) and $\delta F/(pR\mathcal{R}_x^2)\big|_{D=0} = \mathcal{Y}(0, \rho)$ is plotted *versus* $1/\rho$ in the range $1 < \rho < \infty$.

We have checked that our results for arbitrary length ratios ϑ, ρ reduce properly in limiting cases to the forms discussed in Section 2. For example, the location and height of the force maximum given in figure 5 reduce for

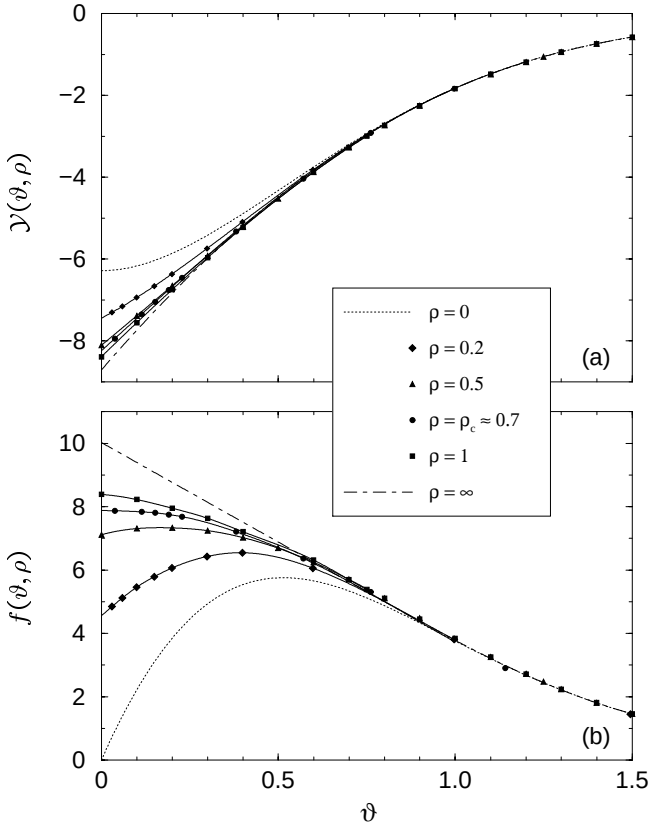

Fig. 4. (a) Scaling function $\mathcal{Y}(\vartheta, \rho) = \delta F/(pR\mathcal{R}_x^2)$ for the free energy of polymer-induced interaction (or potential of mean force) δF between a spherical particle and a wall (see Eq. (2.7)) *vs.* $\vartheta = D/\mathcal{R}_x$ for various fixed values of $\rho = R/\mathcal{R}_x$ ranging from $\rho = \infty$ (lowest curve, Derjaguin approximation (B.9)) to $\rho = 0$ (uppermost curve, small radius expansion (2.2)). The squares, dots, triangles, and diamonds display numerical data. For $\rho < \rho_\mathrm{c} \approx 0.7$ the ϑ-dependence of $\mathcal{Y}$ exhibits a point of inflection which is absent for $\rho > \rho_\mathrm{c}$. (b) Similar representation as in (a) for the scaling function $f(\vartheta, \rho)$ of the polymer-induced force (see equation (2.19)). The points of inflection of $\mathcal{Y}$ in (a) result into *maxima* of f. For $\rho > \rho_\mathrm{c}$ the function $f(\vartheta, \rho)$ is maximum for $\vartheta = 0$ corresponding to a sphere which touches the wall.

$\rho \to 0$ to the correct limiting values that are determined via the small radius expansion in equation (2.2) from the location of and the derivative at the point of inflection of the known half-space profile M_h and from the amplitude A for ideal chains. These limiting values are denoted by SRE (*s*mall R *e*xpansion) in Figure 5.

For a sphere that touches the wall ($D = 0$) the expressions shown in Figures 5b and 6a for the force and the free energy reduce for $\rho \to 0$ to the form $8\pi\,[\zeta(3) + 1/6]\,\rho = 34.4\rho$ and the value $8\pi\zeta(3) = 30.2$, respectively, that follow from equation (2.3) in combination with the upper equation (2.15). Within the region of small ϑ and ρ (*i.e.* $D, R \ll \mathcal{R}_x$) we have not only checked the above mentioned limit $\vartheta/\rho = D/R \to 0$ but also the complete D/R-dependence $Y_3(D/R)$ of $F/(pR^3)$, which is given in equation (2.14). For $D/R = 1$ we have reproduced the value $Y_3(1) = 76.09$ to four digits from extrapolating our

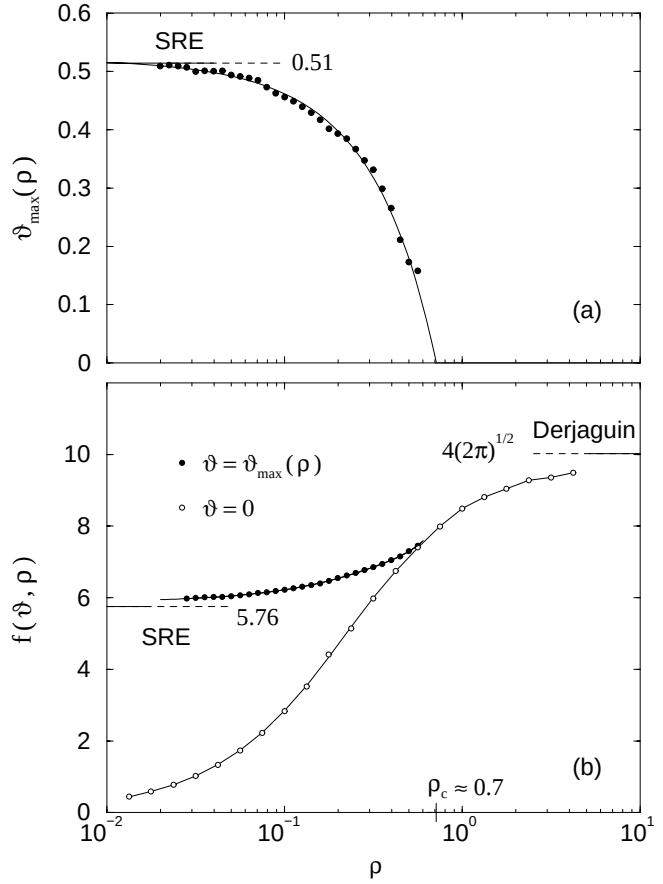

Fig. 5. (a) Scaled particle-wall distance $D_{\max}/\mathcal{R}_x = \vartheta_{\max}(\rho)$ for which the polymer-induced force attains its maximum for fixed R, $\mathcal{R}_x$ and (b) the scaled force at the maximum, $f(\vartheta_{\max}(\rho), \rho)$, *vs.* ρ (upper curve). The horizontal solid lines display the Derjaguin approximation and the small radius expansion (SRE), respectively. The dots display numerical data. The lower curve in (b) is the scaling function $f(0, \rho)$ of the force for a sphere which touches the wall. It coincides with the maximal force for $\rho > \rho_c \approx 0.7$.

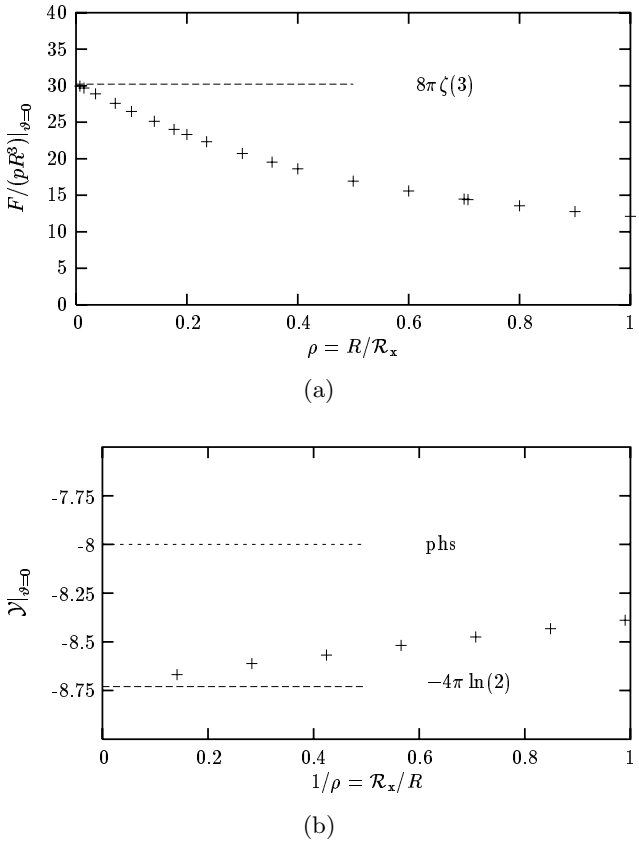

Fig. 6. Free energy for a sphere touching the wall. (a) Scaled free energy cost $F/(pR^3)$ for immersing the particle at $D = 0$ *vs.* ρ. The numerical data (crosses) approach for $\rho \to 0$ the exact value $8\pi\zeta(3)$ (see text). (b) Scaling function $\mathcal{Y}(0, \rho)$ of the free energy of interaction *vs.* $1/\rho$. The data approach for $1/\rho \to 0$ the Derjaguin value $-4\pi \ln 2$ (lower dashed line). The corresponding value -8 (upper dashed line) from the phs-approximation (see text) is clearly ruled out.

numerical results for $1/\rho \equiv \mathcal{R}_x/R = \sqrt{2}\,(40, 80, 160)$ linearly in ρ to $\rho = 0$.

Finally for D, $\mathcal{R}_x \ll R$, *i.e.* for $\rho \to \infty$ and ϑ arbitrary, our numerical results for $\mathcal{Y}$ reduce to the Derjaguin-expression [28] mentioned in equations (2.1, 2.8) and (B.9). In particular the small ϑ limits implied by equation (2.10), $\mathcal{Y}(0, \infty) = -4\pi \ln 2$ and $f(0, \infty) = 4\sqrt{2\pi}$, are approached in Figures 6b and 5b for $1/\rho \to 0$ and $\rho \to \infty$, respectively. Also shown in Figure 6b is the approximation $\mathcal{Y}_{\rm phs}(0, \infty) = -8$ for $\mathcal{Y}(0, \infty)$ that follows from replacing the flexible *p*olymer chain by a non-deformable *h*ard *s*phere (phs-approximation) [4,11]. Its radius is chosen [18,29] as $\sqrt{2/\pi}\mathcal{R}_x$ in order to reproduce the surface free energy of a single large particle or wall, *i.e.* the second term on the right hand side of equation (2.16). Compare also equations (B.6, B.8) below. In terms of the mean square radius of gyration $\mathcal{R}_g^2 = 3\mathcal{R}_{gx}$ of our ideal chain in $d = 3$, the effective phs-radius reads $\sqrt{2/\pi}\mathcal{R}_x = (2/\sqrt{\pi})\mathcal{R}_g$. Our numerical approach is accurate enough to confirm the Derjaguin value and to clearly rule out the phs value. The full ϑ-dependence for $\rho = \infty$ in the phs-approximation,

$$\mathcal{Y}_{\rm phs}(\vartheta, \infty) = \begin{cases} -(2\sqrt{2} - \sqrt{\pi}\vartheta)^2 & \text{for} \quad \vartheta \leqslant 2\sqrt{2/\pi} \\ 0 \end{cases} \tag{4.13}$$

has linear and quadratic terms in ϑ which are *identical* [29] to those in equation (2.10). Thus for $\rho = \infty$ and ϑ not too large the phs-approximation is good, apart from the above mentioned ϑ-independent shift in $\mathcal{Y}$ of about 10%, see Figure 7.

5 Minimizing a Ginzburg-Landau functional

This is another method for investigating ideal chains in the presence of boundaries. It is independent from and complementary to the one in Section 4 and is inspired by the polymer-magnet analogy, compare references [21–23,26,27] and Appendix A.

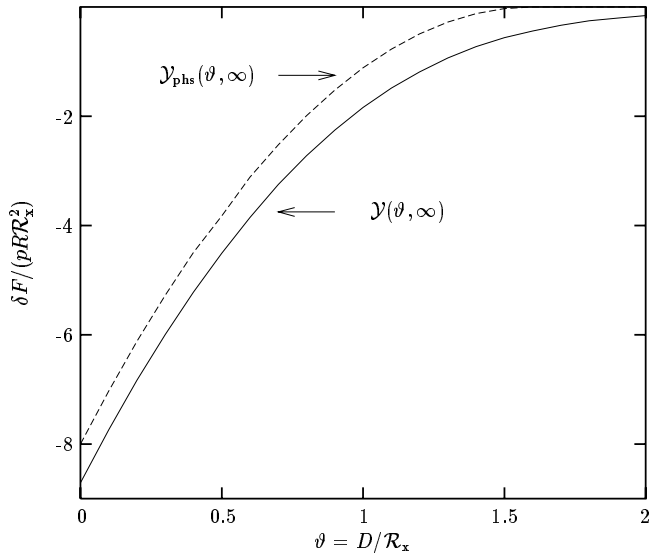

Fig. 7. Scaled free energy for large particle to polymer ratio ρ *vs.* the scaled distance ϑ. Approximating the *p*olymer by a *h*ard *s*phere (phs) leads to the upper curve, see equation (4.13). The exact (Derjaguin) result is the lower curve.

5.1 How to evaluate $\mathcal{E}, \mathcal{M}$ and $\partial F/\partial D$

The Laplace transform

$$\chi(t,\mathbf{r}) = \int_0^\infty \mathrm{d}L\, \mathrm{e}^{-Lt}\, \mathcal{E}(L,\mathbf{r}) \tag{5.1}$$

of the end density $\mathcal{E}$ in case of ideal chains obeys

$$(-\Delta_{\mathbf{r}} + t)\, \chi(t,\mathbf{r}) = 1 \tag{5.2a}$$

for $\mathbf{r}$ inside the available space h\s and vanishes

$$\chi(t, \mathbf{r} \to \sigma) \to 0 \tag{5.2b}$$

as $\mathbf{r}$ approaches the boundary surfaces σ. These relations follow from equations (3.11a–3.11c), respectively. We show in Appendix A that χ is the susceptibility of a Gaussian Ginzburg-Landau model.

It is useful to check the special cases mentioned in Section 4.1. (i) In the unbounded bulk (no boundary) $\chi = \chi_{\rm bulk}$ is $\mathbf{r}$-independent, and equation (5.2a) leads to $\chi_{\rm bulk} = 1/t$, consistent with $\mathcal{E} = \mathcal{E}_{\rm bulk} = 1$. (ii) In the half space the solution $\chi = \chi_{\rm h}(z)$ of (5.2a) that tends to $\chi_{\rm bulk}$ for $z \to \infty$ and vanishes at the wall at $z = 0$ is $\chi_{\rm h} = [1 - \exp(-z\sqrt{t})]/t$. (iii) For a spherical particle in the three-dimensional unbounded space with center at the origin $\chi = \chi_{\rm s}(r) = [1 - (R/r)\exp(-(r-R)\sqrt{t})]/t$. Indeed the inverse Laplace transforms $\mathcal{L}\chi_{\rm h}$ and $\mathcal{L}\chi_{\rm s}$ with $\mathcal{L}$ defined in equation (A3) are identical with the well-known results for $\mathcal{E}_{\rm h}$ and $\mathcal{E}_{\rm s}$ given in Section 4.1. We note that the factor multiplying e^{-Lk^2} in the integral representations of the end density $\mathcal{E}(L,\mathbf{r})$ in Section 4 is essentially given by the imaginary part of the jump of $\chi(t,\mathbf{r})$ across the real t axis at $t = -k^2$. This can be seen directly for $\mathcal{E}_{\rm h}$ and $\mathcal{E}_{\rm s}$. It follows also for the geometry h\s of Figure 1 since equation (5.2) implies that $\chi(t,\mathbf{r})$ can be represented as $\int \mathrm{d}\mathbf{k}\, w(\mathbf{k})\, B(\mathbf{k},\mathbf{r})/(k^2+t)$ in terms of the complete set of eigenfunctions B of the Laplacian $\Delta_{\mathbf{r}}$, see equation (4.9).

Consider $\chi(\mathbf{r})$ for the wall plus sphere geometry of Figure 1. Obviously χ belongs to the class of functions ψ which obey the Dirichlet conditions as in equation (5.2b), vanish inside the particle s, and tend to $\chi_{\rm bulk}$ if z becomes large (with respect to D, R, and $1/\sqrt{t}$) and to $\chi_{\rm h}$ if $r_\parallel$ becomes large. Instead of solving equation (5.2a), we determine $\chi(\mathbf{r})$ as the function $\psi(\mathbf{r})$ which *minimizes* the functional

$$\mathcal{H}\{\psi\} = \int_{\rm h} \mathrm{d}\mathbf{r}\, \mathcal{K}\{\psi\} \tag{5.3}$$

for fixed D, R and $t > 0$, where the integrand has the Ginzburg-Landau form

$$\mathcal{K}\{\psi\} = \frac{1}{2}\left(\nabla_{\mathbf{r}}\psi(\mathbf{r})\right)^2 + \frac{t}{2}\psi^2(\mathbf{r}) - \psi(\mathbf{r})\,. \tag{5.4}$$

Now we show that the free energy F is closely related to the difference

$$\tilde{\mathcal{H}}(D,R,t) = \int_{\rm h} \mathrm{d}\mathbf{r}\, [\mathcal{K}\{\chi\} - \mathcal{K}\{\chi_{\rm h}\}] \tag{5.5}$$

with $\chi_{\rm h}$ the above mentioned half space solution. By partial integration of the $(\nabla\chi)^2$ term in $\mathcal{K}$ and by using equations (5.2a, 5.2b), one finds

$$\tilde{\mathcal{H}}(D,R,t) = -\frac{1}{2}\int_{\rm h} \mathrm{d}\mathbf{r}\, [\chi(\mathbf{r}) - \chi_{\rm h}(z)]\,. \tag{5.6}$$

Both expressions (5.5) and (5.6) suggest that the real quantity $\tilde{\mathcal{H}}$ is non-negative. Comparing equation (5.6) with either equation (3.2) or (E1) shows that the free energy F for ideal chains is related to $\tilde{\mathcal{H}}$ by

$$F = p\,\mathcal{L}\, 2\tilde{\mathcal{H}} \tag{5.7}$$

with the inverse Laplace transform $\mathcal{L}$ defined in equation (A3).

In addition to $\mathcal{E}$ and F, $\mathcal{M}$ can also be obtained from χ. Since $\mathcal{M}(\mathbf{r}) = \mathcal{M}(L,\mathbf{r})$ is proportional to the number of chain conformations with a monomer at $\mathbf{r}$ and since for an ideal chain the latter is [21] proportional to $\int \mathrm{d}\mathbf{r}' \int \mathrm{d}\mathbf{r}'' \int_0^L \mathrm{d}L'\, Z(L';\mathbf{r}',\mathbf{r})\, Z(L-L';\mathbf{r},\mathbf{r}'')$ (see Eq. (3.8)), *i.e.* proportional to the convolution of two end-densities, one finds

$$\mathcal{M}(L,\mathbf{r}) = \frac{1}{L}\int_0^L \mathrm{d}L' \mathcal{E}(L',\mathbf{r})\mathcal{E}(L-L',\mathbf{r}) = \frac{1}{L}\mathcal{L}[\chi(t,\mathbf{r})]^2. \tag{5.8}$$

The prefactor $1/L$ normalizes $\mathcal{M}$ in the bulk.

The force $\partial F/\partial D$ can, in principle, be determined from equation (5.7). However, once χ is known, a more direct and flexible procedure is available, *via* equations (5.12) below. It makes use of the symmetric tensor [40]

$$\mathcal{T}_{j,k}\{\chi\} = (\partial\chi/\partial r_j)(\partial\chi/\partial r_k) - \delta_{j,k}\mathcal{K}\{\chi\}\,, \tag{5.9}$$

with $\mathcal{K}$ from equation (5.4), which due to (5.2a) obeys the continuity equation

$$\sum_k \partial \mathcal{T}_{j,k}\{\chi\}/\partial r_k = 0\,, \quad \mathbf{r} \in \mathrm{h}\backslash\mathrm{s}\,. \tag{5.10}$$

In the absence of the spherical particle s, $\chi = \chi_\mathrm{h}$ and $\mathcal{T}\{\chi_\mathrm{h}\}$ are independent of $\mathbf{r}_\parallel$, and equation (5.10) implies that

$$\mathcal{T}_{j,\perp}\{\chi_\mathrm{h}\} = \delta_{j,\perp}/(2t) \tag{5.11}$$

does not even depend on the distance $r_\perp = z$ from the wall and takes its bulk value. This can be checked by inserting the explicit form of χ_h given above into equation (5.9). Here and below the index $\perp$ denotes the Cartesian index perpendicular to the wall.

We show in Appendix E that

$$\partial F/\partial D = 2p\mathcal{L}\int \mathrm{d}\mathbf{r}_\parallel \left[\mathcal{T}_{\perp,\perp}\{\chi_\mathrm{h}\} - \mathcal{T}_{\perp,\perp}\{\chi\}\right]_{z=0}\,, \tag{5.12a}$$

where the integral runs over the surface $z = 0$ of the wall w. We expect that $\chi_\mathrm{h} \geq \chi$ and that the difference in square brackets is non-negative for all $r_\parallel$ and all $t > 0$, which is consistent with non-negative $\partial F/\partial D$ for all $\mathcal{R}_x^2 = 2L$. Together with equation (5.8) for the monomer density the expression (5.12a) or (E5) for the force confirms the density-force relation (3.4) for ideal chains, taking into account $\chi(r_\parallel, z) \to z[\partial_z\,\chi(r_\parallel, z)]_{z=0}$ and $\mathcal{L}(\partial_z\,\chi_\mathrm{h})^2 \to 1$ close to the wall. Since the difference in the square brackets in (5.12a) is negligible far away from the particle s, one can extend the integration in (5.12a) to a closed surface by adding the surface of a large hemisphere in the half-space h with center at the origin. One then finds

$$\partial F/\partial D = 2p\mathcal{L}\sum_k \int_{\tilde{S}} \mathrm{d}\tilde{S}_k\,\mathcal{T}_{\perp,k}\{\chi\}\,, \tag{5.12b}$$

where $\tilde{S}$ is a closed surface surrounding the spherical particle s in the half space h and the vector $\mathrm{d}\mathbf{S}$ normal to $\tilde{S}$ points outward. Note that we have dropped $\mathcal{T}_{\perp,k}\{\chi_\mathrm{h}\}$ in (5.12b), since it is space-independent and does not contribute. Due to the continuity equation (5.10), the value of the surface integral in (5.12b) is independent of the shape of $\tilde{S}$. This provides an important check on the accuracy of the numerical method for calculating $\chi(\mathbf{r})$. We considered several *spherical* integration surfaces $\tilde{S}$ of different radii surrounding the particle s.

Before embarking in Section 5.2 on the general case it is instructive to reproduce with our approach the known result for a *small* sphere near a wall with $R \ll D$, $1/\sqrt{t}$. In this case [18]

$$\chi(\mathbf{r}) - \chi_\mathrm{h}(\mathbf{r}) \equiv \delta\chi = -2A_\mathrm{id}R^{d-2}\,\chi_\mathrm{h}(z_\mathrm{s})G_\mathrm{h}(\mathbf{r}_\mathrm{s}, \mathbf{r})\,, \tag{5.13}$$

where A_id is defined below equation (2.2), $\mathbf{r}_\mathrm{s} = (\mathbf{r}_{\mathrm{s}\parallel}, z_\mathrm{s})$ is the location of the center of the spherical particle, and

$$G_\mathrm{h}(\mathbf{r}_s, \mathbf{r}) = \int \frac{\mathrm{d}^{d-1}\mathbf{p}}{(2\pi)^{d-1}}\,\mathrm{e}^{\mathrm{i}\mathbf{p}(\mathbf{r}_{\mathrm{s}\parallel} - \mathbf{r}_\parallel)} \times \frac{1}{2\kappa}\left[\mathrm{e}^{-\kappa|z_\mathrm{s}-z|} - \mathrm{e}^{-\kappa(z_\mathrm{s}+z)}\right] \tag{5.14}$$

is a correlation function of the Ginzburg-Landau model in the half-space with $\kappa = \sqrt{p^2 + t}$, compare references [24–26]. To first order in $\delta\chi$ this leads to

$$\mathcal{T}_{\perp,\perp}\{\chi_\mathrm{h} + \delta\chi\} - \mathcal{T}_{\perp,\perp}\{\chi_\mathrm{h}\} = [(\partial_z\chi_\mathrm{h})\partial_z - \chi_\mathrm{h}t + 1]\delta\chi\,. \tag{5.15}$$

Since on the rhs of (5.15) only the derivative-term contributes for $z = 0$, the rhs of (5.12a) becomes $pA_\mathrm{id}R^{d-2}\mathcal{R}_x^2\,\partial_{z_\mathrm{s}}\,\mathcal{M}_\mathrm{h}$, which is consistent with equation (2.2). Here in the last step we used $2L = \mathcal{R}_x^2$ (Eq. (3.9)) and related χ_h^2 to $\mathcal{M}_\mathrm{h}$ by means of equation (5.8).

5.2 Numerical method and results for $\mathcal{M}$ and $\partial F/\partial D$

In general the configuration $\chi(\mathbf{r})$ that minimizes the GL functional $\mathcal{H}\{\psi\}$ in (5.3) can only be determined numerically and for real and positive values of t. Here we use the standard numerical method of steepest descent [41]. For the numerical implementation we use a bispherical coordinate lattice which is obtained by a conformal transformation from a concentric lattice [31,32]. The concentric lattice is bounded by two concentric spherical surfaces which are mapped onto the surfaces of the wall and of the spherical particle by the conformal transformation. We approximate $\psi(\mathbf{r})$ by a cubic spline interpolation between its values ψ_i at the lattice sites which are the degrees of freedom of the numerical minimization procedure [42].

After minimization of $\mathcal{H}\{\psi\}$ yielding $\chi(\mathbf{r})$, the end density $\mathcal{E}(\mathbf{r})$ and the monomer density $\mathcal{M}(\mathbf{r})$ are inferred from equations (5.1, 5.8), respectively, by carrying out the inverse Laplace transform $\mathcal{L}$. The effective force $\partial F/\partial D$ on the sphere can be calculated *via* equation (5.12b). The derivatives of χ with respect to the spatial coordinates as needed for the stress tensor (5.9) are available at the lattice sites from the spline interpolation (see the previous paragraph). A further spline interpolation yields the stress tensor as a continuous function on different spherical surfaces $\tilde{S}$ surrounding the particle. Since the result of the integration in equation (5.12b) should be independent of $\tilde{S}$ we stopped the minimization procedure as soon as the relative deviations between the results obtained from the different spherical surfaces did not exceed 1 %.

A central step in the evaluation of $\mathcal{E}$, $\mathcal{M}$ and $\partial F/\partial D$ is to analytically continue to complex t in order to perform the inverse Laplace transform $\mathcal{L}$. This can be done by means of an appropriate Padé interpolation scheme.

We have used the present method to calculate for given $\vartheta = D/\mathcal{R}_x$ and $\rho = R/\mathcal{R}_x$ both the force $\partial F/\partial D$ on the sphere and the depletion hole in the normalized monomer density $[\mathcal{M}(\mathbf{r})/\mathcal{M}_\mathrm{h}(z)]^{(\mathrm{as})}$ near the wall that is induced by

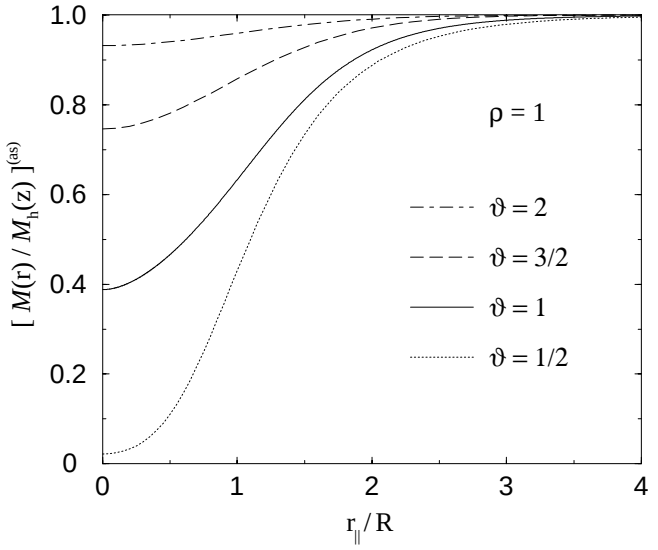

Fig. 8. Reduction in the normalized monomer density near the wall $[\mathcal{M}(\mathbf{r})/\mathcal{M}_{\rm h}(z)]^{(\rm as)}$ due to the presence of the spherical particle, plotted as a function of $r_\parallel/R$ for $\rho = R/\mathcal{R}_x = 1$ and various values of $\vartheta = D/\mathcal{R}_x$ (compare Fig. 1). The curves have been calculated numerically by minimizing the GL functional in equation (5.3) and by using equation (5.8). According to the density force relation (3.4) the integral of $1-[\mathcal{M}(\mathbf{r})/\mathcal{M}_{\rm h}(z)]^{(\rm as)}$ over $\mathbf{r}_\parallel$ yields the force on the sphere. For $\rho = 1 > \rho_{\rm c}$ the relative reduction becomes more pronounced, and hence the force increases, as the sphere moves towards the wall, *i.e.* as ϑ is decreased (compare Eq. (2.19) and Fig. 4b).

the presence of the sphere and that enters the density force relation (3.4). Figure 8 shows the results for the monomer density for the case $\rho = 1$ in which the depletion hole and the force increase monotonically with decreasing ϑ .

We have checked (3.4) for the numerically calculated curves shown in Figure 8 and found that the relative differences between the lhs and rhs of (3.4) do not exceed 1 %. The corresponding values of the scaling function $f(\vartheta,\rho)$ for the force in equation (2.19), $f(2,1) = 0.42$, $f(\frac{3}{2},1) = 1.45$, $f(1,1) = 3.92$, and $f(\frac{1}{2},1) = 6.79$ check with the same accuracy also with the corresponding results for f obtained in Section 4, see Figure 4b.

6 Summary and concluding remarks

We have investigated the attractive depletion-interaction between a spherical particle and the planar boundary wall in a dilute solution of long flexible free nonadsorbing polymer chains. For the simple case of *ideal* chains we have evaluated the free energy of polymer-induced interaction δF for *arbitrary* ratios of the three relevant mesoscopic lengths polymer size $\mathcal{R}_x$, particle radius R, and particle-wall distance D, compare Figure 1. We found that the D-variation of δF depends crucially on the particle to polymer size ratio $\rho = R/\mathcal{R}_x$, compare Figure 4. We also evaluated the normalized densities $\mathcal{E}$ and $\mathcal{M}$ of chain-ends and chain-monomers, compare Figures 3 and 8. The densities can, in principle, also be observed experimentally and are related to δF in a fundamental way, see equations (3.2, 3.4).

Since on the mesoscopic scales considered $\delta F/kT$, $\mathcal{E}$, and $\mathcal{M}$ do not depend on microscopic details, we chose a particularly convenient model, in which the polymers are described by continuous Brownian chains or random walks subject to potential barriers of infinite height at the surfaces of the particle and the wall. In this model $\mathcal{E}$ satisfies a diffusion equation with Dirichlet boundary conditions, see equation (3.11).

Here we summarize our main results. We used the following two independent methods to obtain numerical results for δF, $\mathcal{E}$, and $\mathcal{M}$:

(1) Solving the diffusion equation with boundary and "initial" conditions for $\mathcal{E}$, see equation (3.11), by superposing eigenfunctions of the Laplacian $\Delta_{\mathbf{r}}$. This method is described in Sections 4.1 and 4.2.

(2) Evaluating the Laplace transform of $\mathcal{E}$ by minimizing a Ginzburg-Landau functional, compare Section 5.1. This method allows one, in particular, to calculate $\mathcal{M}$. Equations (5.1–5.4) show in an elementary way how the basic relation for method (2) follows from that of method (1) and constitute one of the simplest examples of a polymer-magnet analogy.

The two methods are complementary: While method (1) works best if the polymer size $\mathcal{R}_x$ is of the order of the geometrical lengths D and R or *larger* (see the first paragraph in Sect. 4.3), minimizing the Ginzburg-Landau functional in method (2) is easy if the correlation length ξ, and thus $\mathcal{R}_x$, is of the order of the geometrical lengths or *smaller*.

The following numerical results were obtained:

(3) The dependence of $\mathcal{E}$ on $r_\parallel$ and z (see Fig. 1) is shown in Figures 3a-c for a particle to polymer size ratio $R/\mathcal{R}_x = 1/4$ and $D/R = 1, 3, 5$. Note the increase of the difference $\mathcal{E}_{\rm h} - \mathcal{E}$ between the densities in absence and presence of the particle as the distance D increases in Figure 3a to Figure 3c. This leads *via* equation (3.2) to a corresponding increase of the free energy F of immersing the particle, and thus to the attractive depletion-interaction.

(4) Calculating $\mathcal{E}$ for a wide range of $\rho = R/\mathcal{R}_x$ and $\vartheta = D/\mathcal{R}_x$ leads to the results shown in Figures 4a, 4b for the scaling functions $\mathcal{Y}$ and f of δF and the polymer-induced force $\partial\delta F/\partial D$, respectively (see Eqs. (2.7, 2.19)). While for large particle to polymer size ratio $\rho > \rho_{\rm c} \approx 0.7$ the force decreases *monotonically* with increasing D, for $\rho < \rho_{\rm c}$ the D-dependence of δF and the force has a point of inflection and a *maximum*, respectively, compare Figures 4 and 5. Results for the special case $D = 0$ in which the particle *touches* the wall are shown in Figures 5b and 6. We have checked that the numerically determined curves in Figure 4 approach the known behavior in the four limits (i)-(iv) mentioned in Section 2, see the discussion in Section 4.4. We note, in particular, the limit $\rho \to \infty$ (limit (i) in Sect. 2) in which the behavior (B.9) of the Derjaguin-approximation is approached. It is shown in Figure 7 that several, but not all, features of this behavior are reproduced by approximating [4,11] the *p*olymer by a *h*ard *s*phere (phs-approximation).

(5) The depletion of the monomer density $\mathcal{M}$ close to the wall is shown in Figure 8 for a size ratio $\rho = 1$ and various values of the scaled particle-wall distance ϑ. We have checked that our numerical results approach the known behavior (3.5) and (3.6), respectively, in the limits (ii) and (iv) mentioned in Section 2.

(6) The force $\partial\delta F/\partial D$ was calculated numerically also by means of the stress tensor of the Ginzburg-Landau model using equations (5.9, 5.12b). We checked these results for the force both by integrating the monomer density in (5) according to the density-force relation (3.4) and by comparing with the results from method (1). In all cases the relative differences do not exceed 1%.

Finally we summarize our new analytical results.

(7) In the large polymer limit $\mathcal{R}_x \to \infty$ (denoted by (iii) in Sect. 2) the free energy F of immersing the particle remains finite and has the form given by equations (2.3, 2.14) as we show in Appendix D. For large $\mathcal{R}_x$ the particle is like a point-defect on the wall, whose strength depends on R and D. Compare equation (D1).

(8) For $\mathcal{R}_x \ll D$ (denoted as region (iv) in Sect. 2) the scaling functions f and $\mathcal{Y}$ of the force and δF (see Eqs.(2.7, 2.19)) are independent of the size ratio ρ, while the density profiles $\mathcal{M}$ and $\mathcal{E}$ near the wall have the forms (3.6) and (C10), respectively, as we show in Appendix C.

It would be interesting to extend this work in the following directions :

(a) Including the effective monomer-monomer repulsion for polymer chains in the good solvent region: Then the scaling function $\mathcal{Y}(\vartheta, \rho)$ in three dimensions in equation (2.7) is different from Figure 4a. While $\mathcal{Y}$ is again expected to approach a *finite* function $Y_1(\vartheta)$ for $\rho \to \infty$, for $\rho \to 0$ it is given by $\rho^{2-1/\nu} Y_2(\vartheta)$, where Y_2 is a function with an inflection point, and approaches *zero*, *i.e.* the *horizontal axis* in a plot corresponding to Figure 4a, since now ν is larger than 1/2.

(b) Higher polymer concentration: Both the cases of small nonvanishing overlap between chains (virial expansion) and of strong overlap (semi-dilute polymer solution) are of interest. It is still unknown whether or not overlapping flexible polymer chains can lead to a depletion *repulsion* [43] between particles.

(c) Depletion interaction between two (or more) particles: Methods (1) and (2) can be extended to two spherical particles with equal radii R and with arbitrary ratios of the three lengths R, $\mathcal{R}_x$ and distance between the particles. This would generalize previous studies of small and large particle to polymer size ratios, see [30], and check to what extent simulations [15,16] probe the universal scaling region.

We thank T.W. Burkhardt for useful discussions and a critical reading of the manuscript. The work of A. H. has been supported by the German Science Foundation through Sonderforschungsbereich 237 *Unordnung und große Fluktuationen.*

Appendix A: Polymer-magnet analogy

In order to introduce the field-theory notation necessary for Appendices B-E and to make the paper more self-contained, we here briefly sketch the well known polymer-magnet analogy. More extensive discussions can be found in references. [18,21–23,26,27].

The statistics of long flexible polymers is closely related to a Ginzburg-Landau (GL) field theory with a fluctuating n-component order-parameter field $\boldsymbol{\Phi} = (\Phi_1, \ldots, \Phi_n)$. The field $\boldsymbol{\Phi}$ *vanishes* (Dirichlet condition) on the nonadsorbing surfaces σ of the wall w and the particle s and is governed by the probability $\sim \exp(-H\{\boldsymbol{\Phi}\})$, with

$$H = \int_{\mathrm{h}\backslash\mathrm{s}} \mathrm{d}\mathbf{r} \left[\left(\sum_{j=1}^{n} K\{\Phi_j\} \right) + K_{\mathrm{int}}(\boldsymbol{\Phi}^2(\mathbf{r})) \right], \qquad \text{(A.1)}$$

where

$$K\{\Phi\} = \frac{1}{2} \left(\nabla_{\mathbf{r}} \Phi(\mathbf{r})\right)^2 + \frac{t}{2} \Phi^2(\mathbf{r}) \qquad \text{(A.2)}$$

is bilinear in $\boldsymbol{\Phi}$ while $K_{\mathrm{int}} \sim (\boldsymbol{\Phi}^2)^2$. Field theories of this type have been used to study boundary critical phenomena [24,25]. The expansion of polymer quantities with respect to the excluded volume interaction between monomers follows term by term from the expansion of correlation functions of the field theory with respect to K_{int} by means of the formal limit $n \to 0$ and the inverse Laplace transform

$$\mathcal{L} = \mathcal{L}_{t \to L} = \frac{1}{2\pi \mathrm{i}} \int_{\mathcal{P}} \mathrm{d}t \, \mathrm{e}^{Lt} \, . \qquad \text{(A.3)}$$

Here $\mathcal{P}$ is an integration path in the complex t-plane to the right of all singularities of the quantity onto which $\mathcal{L}$ is applied. The Laplace conjugate L of t is related to $\mathcal{R}_x$. For example, the end density $\mathcal{E}$ defined in equation (3.8) is given by [18,21–23,26,27]

$$\mathcal{E}(\mathbf{r}_A) = \zeta_{\mathrm{bulk}}^{-1} \, \mathcal{L} \int_{\mathrm{h}\backslash\mathrm{s}} \mathrm{d}\mathbf{r}_B \, \langle \varphi_{A,B} \rangle \, , \qquad \text{(A.4)}$$

where

$$\zeta_{\mathrm{bulk}} = \mathcal{L} \int \mathrm{d}\mathbf{r}_B \, \langle \varphi_{A,B} \rangle_{\mathrm{bulk}} \qquad \text{(A.5)}$$

and we introduce the compact notation

$$\varphi_{A,B} = \Phi_1(\mathbf{r}_A) \, \Phi_1(\mathbf{r}_B) \, . \qquad \text{(A.6)}$$

Here and below $\langle\,\rangle$, $\langle\,\rangle_{\mathrm{h}}$ and $\langle\,\rangle_{\mathrm{bulk}}$ denote averages in the half space and outside the sphere (Fig. 1), in the half space, and in the unbounded space in the limit $n \to 0$ mentioned above.

For an *ideal* polymer chain the density-density (excluded-volume) interaction K_{int} *vanishes*, and the GL field theory decouples into n independent Gaussian field theories. Thus the averages in (A.4) and (A.5) reduce

to one-component Gaussian averages. The first average, $\langle\varphi_{A,B}\rangle^{(\mathrm{Gauss})} \equiv G(t,\mathbf{r}_A,\mathbf{r}_B)$, satisfies the Schrödinger-type equation [21,18]

$$(-\Delta_{\mathbf{r}_A} + t)\; G(t,\mathbf{r}_A,\mathbf{r}_B) \;=\; \delta(\mathbf{r}_A - \mathbf{r}_B) \qquad \text{(A.7a)}$$

for $\mathbf{r}_A$ and $\mathbf{r}_B$ in h\s and the Dirichlet boundary condition

$$G(t,\mathbf{r}_A,\mathbf{r}_B) \;\to\; 0 \qquad \text{(A.7b)}$$

for $\mathbf{r}_A$ or $\mathbf{r}_B$ approaching the surface σ of either wall or particle. The Gaussian susceptibility

$$\chi(\mathbf{r}_B) \;\equiv\; \chi(t,\mathbf{r}_B) \;=\; \int_{\mathrm{h\backslash s}} \mathrm{d}\mathbf{r}_A\, G(t,\mathbf{r}_A,\mathbf{r}_B) \qquad \text{(A.8)}$$

then satisfies equation (5.2), $\zeta_{\mathrm{bulk}} = \mathcal{L}\,1/t = 1$, and equation (A.4) reduces to equation (5.1). The normalized partition function $Z(L,\mathbf{r}_A,\mathbf{r}_B)/\int \mathrm{d}\mathbf{r}_A\, Z_{\mathrm{bulk}}(L,\mathbf{r}_A,\mathbf{r}_B)$ in equation (3.8) equals $\mathcal{L}G(t,\mathbf{r}_A,\mathbf{r}_B)$.

Appendix B: Derjaguin approximation

Consider a particle with the shape of a *plate* p oriented parallel to the wall w, with lateral area $\mathcal{A} = l^{d-1}$, width $\mathcal{W}$ and closest surface-to-surface distance from the wall $\mathcal{D}$. We assume that $\mathcal{R}_x \ll l$. Then the free energy of interaction per unit area is

$$\frac{1}{\mathcal{A}}\,\delta F_{\mathrm{p\|w}} \to p\,\delta\mathcal{F}(\mathcal{D},\mathcal{R}_x)\;, \qquad \text{(B.1)}$$

where $\delta\mathcal{F}$ is independent of $\mathcal{A}$ and $\mathcal{W}$ and has the dimension of a length.

For a large spherical particle with $\mathcal{R}_x, D \ll R$ the Derjaguin approximation [28] for the free energy

$$\delta F \to p \int \mathrm{d}\mathbf{r}_\| \;\delta\mathcal{F}(\widetilde{D}(r_\|),\mathcal{R}_x) \qquad \text{(B.2)}$$

with $\delta\mathcal{F}$ from (B.1) and $\widetilde{D}$ from equation (3.7b) is expected to be exact. Since the R-dependence is entirely in $\widetilde{D}$, the integral in (B.2) is proportional to $R^{\frac{d-1}{2}}$. The overall length dimension of the integral is $(\mathrm{length})^d$ and leads to the form (2.1) of δF.

Applying equation (3.2) to the case of the plate, one can express the free energy per unit area $F_{\mathrm{p\|w}}/\mathcal{A}$ needed to insert the plate near the wall as

$$p\mathcal{F} = p[\mathcal{W} + (1-U)\mathcal{D}] \qquad \text{(B.3)}$$

in terms of the average

$$U = \frac{1}{\mathcal{D}}\int_0^{\mathcal{D}} \mathrm{d}z\,\mathcal{E}_{\mathrm{p\|w}}(\mathbf{r}_\| \in \mathrm{slit}, z) \qquad \text{(B.4)}$$

of the bulk-normalized density $\mathcal{E}_{\mathrm{p\|w}}(\mathbf{r})$ of chain ends in the space between the wall and the plate. Our assumption $\mathcal{R}_x \ll l$ implies that the density in this region is independent of $r_\|$ and $\mathcal{W}$. Note that the density $\mathcal{E}_{\mathrm{p\|w}}(\mathbf{r})$ with $\mathbf{r}$ between the wall and the plate equals the ratio of the partition function of a chain with a fixed end at $\mathbf{r}$ to the partition function of a chain with fixed end in the bulk. The width $\mathcal{W}$ in (B.3) drops out from the difference in (B.1), *i.e.*

$$\delta\mathcal{F} = \mathcal{F} - \lim_{\mathcal{D}\to\infty}\mathcal{F} = (1-U)\mathcal{D} - 2\mathcal{I} \qquad \text{(B.5)}$$

with

$$\mathcal{I} = \int_0^\infty \mathrm{d}z\,[\,1 - \mathcal{E}_{\mathrm{h}}(z)\,]\,. \qquad \text{(B.6)}$$

Here $\mathcal{E}_{\mathrm{h}}$ is the bulk-normalized density of chain ends in the half space and the integral $\mathcal{I}$ equals the surface free energy per unit area and pressure of its planar boundary. For the case $\mathcal{D} = 0$ note the obvious result that $\delta\mathcal{F}(0,\mathcal{R}_x)$ equals $-2\mathcal{I}$. In $d = 3$, equation (B.2) implies that δF equals $2\pi pR\int_D^\infty \mathrm{d}\mathcal{D}\;\delta\mathcal{F}(\mathcal{D},\mathcal{R}_x)$. In particular, the modulus $(\partial\delta F/\partial D)_{D=0}$ of the force acting on a large spherical particle that touches the wall equals $4\pi pR\mathcal{I}$.

Simple explicit expressions can be obtained for *ideal* chains. Calculating the density $\mathcal{E}_{\mathrm{p\|w}}$ between the plate and the wall, *e.g.* by means of the method in equations (5.1, 5.2), one finds

$$\delta\mathcal{F} = -\mathcal{L}\,\frac{4}{t^{3/2}}\,\frac{1}{1+\exp(\mathcal{D}\sqrt{t})} \qquad \text{(B.7)}$$

and

$$\mathcal{I} = \mathcal{L}\,t^{-3/2} = \sqrt{2/\pi}\,\mathcal{R}_x\;, \qquad \text{(B.8)}$$

where the inverse Laplace transform $\mathcal{L}$ is defined in equation (A.3). Inserting (B.7) into (B.2) and setting $d = 3$, one finds that the function in equation (2.8) is given by [29]

$$\mathcal{Y}(\vartheta,\infty) = -4\pi\int_{\mathcal{P}}\frac{\mathrm{d}\tau}{2\pi\mathrm{i}}\,\mathrm{e}^\tau\,\tau^{-2}\ln[1+\exp(-\vartheta\sqrt{2\tau})] \qquad \text{(B.9)}$$

with an integration path $\mathcal{P}$ similar to (A.3). Equation (B.9) implies the limiting behavior (2.10) and (2.12).

Appendix C: The regime $\mathsf{D} \gg \mathcal{R}_\mathsf{x}$

Here we derive for the geometry of Figure 1 the leading behavior of the Gaussian two-point function G in equation (A.7) for large D/ξ and *arbitrary* R/ξ where $\xi = t^{-1/2}$ is the correlation length. *Via* the polymer magnet analogy described in Appendix A this yields the leading behavior of ideal chain quantities for large $D/\mathcal{R}_x$ with arbitrary $R/\mathcal{R}_x$.

We introduce the Gaussian two-point correlation function $G_{\mathrm{s}}(\mathbf{r}_1,\mathbf{r}_2)$ for the outer space $\mathbf{R}^d$\s of the spherical particle s in the *bulk*, *i.e.* in the absence of the wall, and the corresponding correlation function $G_{\bar{\mathrm{s}}}(\mathbf{r}_1,\mathbf{r}_2)$ for the particle $\bar{\mathrm{s}}$ which is the mirror image of s w.r.t. the surface $z = 0$ of w as in Figure 2. Below we shall argue that

$$G(t,\mathbf{r}_A,\mathbf{r}_B) \;\to\; \widetilde{G}(t,\mathbf{r}_A,\mathbf{r}_B)\;,\quad D/\xi\to\infty\;, \qquad \text{(C.1)}$$

where

$$\widetilde{G}(\mathbf{r}_A,\mathbf{r}_B) \,=\, G_{\rm s}(\mathbf{r}_A,\mathbf{r}_B) \\ -\,[G_{\rm s}(\mathbf{r}_A,\bar{\mathbf{r}}_B) \,+\, G_{\bar{\rm s}}(\mathbf{r}_A,\bar{\mathbf{r}}_B) \,-\, G_{\rm bulk}(\mathbf{r}_A,\bar{\mathbf{r}}_B)]\,. \quad \text{(C.2)}$$

Here $\bar{\mathbf{r}}_B$ is the mirror image of $\mathbf{r}_B$.

Obviously the rhs of equation (C.2) containing only *single*-particle contributions is much easier to calculate than the full G. The validity of equation (C.1) can be seen as follows: (i) $\widetilde{G}$ fulfills equation (A.7a); (ii) $\widetilde{G}$ is symmetric in $\mathbf{r}_A$ and $\mathbf{r}_B$; (iii) the boundary condition (A.7b) on the surfaces of w and s is violated only weakly, *i.e.*, only at the order of $\exp(-2D/\xi)$. For large D/ξ this correction can be neglected w.r.t. the order $\exp(-D/\xi)$ of the effective interaction between w and s. In order to check (iii) one may consider the behavior of $\widetilde{G}$ for each of the four cases that $\mathbf{r}_A$ or $\mathbf{r}_B$ is located on the surface of w or s.

For example, for $\mathbf{r}_B$ on the surface $\sigma_{\rm w}$ of w the sum of the first two terms on the rhs of (C.2) vanishes and

$$\widetilde{G}(\mathbf{r}_A,\mathbf{r}_B) \,\to\, -\,g_{\bar{\rm s}}(\mathbf{r}_A,\bar{\mathbf{r}}_B), \quad \mathbf{r}_B \in \sigma_{\rm w} \qquad \text{(C.3)}$$

where

$$g_{\bar{\rm s}}(\mathbf{r}_1,\mathbf{r}_2) \,=\, G_{\bar{\rm s}}(\mathbf{r}_1,\mathbf{r}_2) \,-\, G_{\rm bulk}(\mathbf{r}_1,\mathbf{r}_2) \qquad \text{(C.4)}$$

is the deviation from the bulk correlation function that arises from the presence of $\bar{\rm s}$. Thus the rhs of equation (C.3) has the negligible order of magnitude of $\exp(-2D/\xi)$ of the product of two bulk correlation functions which extend over the distances, not smaller than D, from $\bar{\mathbf{r}}_B$ (located at $\sigma_{\rm w}$) and $\mathbf{r}_A$, respectively, to the surface of $\bar{\rm s}$. Compare Figure 2.

The three other cases mentioned above can be examined along similar lines.

Now we use equation (C.1) to evaluate the densities $\mathcal{E}$ and $\mathcal{M}$ of ends and monomers near the wall. They can be obtained from the expansion about the wall,

$$\chi(\mathbf{r}_B) \,=\, z_B\, a(r_{B\|}) \,+\, \mathcal{O}({z_B}^2), \qquad \text{(C.5)}$$

of the susceptibility in equation (A.8). Calculating $\chi(\mathbf{r}_B)$ becomes quite simple if $\mathbf{r}_B$ is near the wall. First, the sum $g_{\bar{\rm s}}(\mathbf{r}_A,\bar{\mathbf{r}}_B)$ of the two last terms on the rhs of (C.2) can be neglected in this case as argued below equation (C.4) and

$$\chi(\mathbf{r}_B) \,\to\, \int_{\rm h\setminus s} {\rm d}\mathbf{r}_A\,[\,G_{\rm s}(\mathbf{r}_A,\mathbf{r}_B) \,-\, G_{\rm s}(\mathbf{r}_A,\bar{\mathbf{r}}_B)\,]. \qquad \text{(C.6)}$$

Second, the integral on the rhs of equation (C.6) can be replaced by simpler ones since for $\mathbf{r}_B$ near the wall

$$\int_{\rm h\setminus s} {\rm d}\mathbf{r}_A\, G_{\rm s}(\mathbf{r}_A,\mathbf{r}_B) \,-\, \int_{\rm h} {\rm d}\mathbf{r}_A\, G_{\rm bulk}(\mathbf{r}_A,\mathbf{r}_B) \\ \to \int_{\mathbf{R}^d\setminus {\rm s}} {\rm d}\mathbf{r}_A\, G_{\rm s}(\mathbf{r}_A,\mathbf{r}_B) \,-\, \int_{\mathbf{R}^d} {\rm d}\mathbf{r}_A\, G_{\rm bulk}(\mathbf{r}_A,\mathbf{r}_B) \\ =\, \chi_{\rm s}(\mathbf{r}_B) \,-\, \chi_{\rm bulk}. \qquad \text{(C.7)}$$

The reason is that the difference $g_{\rm s}(\mathbf{r}_A,\mathbf{r}_B)$ of the two integrands is negligible for $\mathbf{r}_B$ near the wall if $\mathbf{r}_A$ is outside h. From equations (C.6, C.7) the coefficient $a(r_\|)$ in (C.5) follows as

$$a(r_\|) \,=\, 2\,[\,\partial_z \int_{\rm h} {\rm d}\mathbf{r}_A\, G_{\rm bulk}(\mathbf{r}_A,\mathbf{r})\,]_{z=0} \,-\, \alpha(r_\|)\,, \qquad \text{(C.8)}$$

where α is given by

$$\alpha(r_\|) \,=\, -\,2\,[\,\partial_z\,\chi_{\rm s}(\mathbf{r})\,]_{z=0} \\ =\, -\,\frac{\rm d}{{\rm d}(r_{\rm sw}^2)}\,\frac{4R(R+D)}{t\,r_{\rm sw}}\,\exp[-(r_{\rm sw}-R)\sqrt{t}\,], \qquad \text{(C.9)}$$

apart from terms of negligible order of $\exp(-2D/\xi)$. Here $r_{\rm sw}$ is defined as in equation (3.6b). In the last step of equation (C.9) we have used the explicit form of $\chi_{\rm s}(\mathbf{r})$ in three dimensions for the present situation of a particle centered at $\mathbf{r}_{\rm s} = (\mathbf{0}, D+R)$ which follows from the form given below equation (5.2) for a particle with center at the origin. While the first term on the rhs of equation (C.8) equals $[\,\partial_z\chi_{\rm h}(\mathbf{r})\,]_{z=0}$, *i.e.* the coefficient $a = t^{-1/2}$ in the absence of the particle, $\alpha(r_\|)$ is the reduction of $a(r_\|)$ from the presence of the particle s. It determines *via* equations (5.1, 5.8) the relative reduction near the wall of the density of chain ends,

$$1 - [\,\mathcal{E}(\mathbf{r})\,/\,\mathcal{E}_{\rm h}(z)\,]^{\rm (as)} \,\to\, \mathcal{L}\,\alpha(r_\|)\,/\,\mathcal{L}\,t^{-1/2} \\ \to\, 2\,\frac{R\,(R+D)}{(r_{\rm sw})^2}\,\exp\left[-\,\frac{(r_{\rm sw}-R)^2}{2\mathcal{R}_x^2}\right], \\ \text{for} \quad D/\mathcal{R}_x \to \infty\,, \qquad \text{(C.10)}$$

with the second line applying in three dimensions, and of the density of chain monomers,

$$1 - [\,\mathcal{M}(\mathbf{r})\,/\,\mathcal{M}_{\rm h}(z)\,]^{\rm (as)} \,\to\, 2\,\mathcal{L}\,t^{-1/2}\,\alpha(r_\|)\,, \qquad \text{(C.11)}$$

with the explicit form in three dimensions given in equation (3.6a).

The force is obtained from equations (C.9, C.11) by means of the density force relation (3.4). In three dimensions the surface element ${\rm d}\mathbf{r}_\| = {\rm d}^2 r_\|$ in the corresponding integral, $\int {\rm d}\mathbf{r}_\|\,\alpha(r_\|)$, equals $\pi{\rm d}(r_{\rm sw})^2$ and the integration over the complete differential α in equation (C.9) is trivial and leads for the force in three dimensions to the simple *linear* R-dependence,

$$\partial F/\partial D \,\to\, p\,R\,8\pi\,\mathcal{L}\,t^{-3/2}\,\exp(-D\sqrt{t})\ ,\ D/\mathcal{R}_x \,\to\, \infty\,, \qquad \text{(C.12)}$$

for arbitrary R, which implies equation (2.12).

Alternatively, the force can be calculated without recourse to the density force relation, by inserting (C.1) into the free energy expression (E1) and differentiating w.r.t. D. Since in each of the contributions D enters only the integration boundary, and not the integrand, the differentiation places one of the two integration variables onto the surface of the wall, *e.g.*

$$\partial_D \int_{\rm h\setminus s} {\rm d}\mathbf{r}_A \int_{\rm h\setminus s} {\rm d}\mathbf{r}_B\; g_{\rm s}(\mathbf{r}_A,\mathbf{r}_B) \\ =\, 2\int {\rm d}\mathbf{r}_{B\|} \int_{\rm h\setminus s} {\rm d}\mathbf{r}_A\; g_{\rm s}(\mathbf{r}_A,(\mathbf{r}_{B\|},0))\,, \qquad \text{(C.13)}$$

and one can proceed similarly as in equation (C.7). This leads to

$$\partial F/\partial D \to 4\,p\,\mathcal{L}\int \mathrm{d}\mathbf{r}_\parallel\,[\,\chi_{\rm bulk}-\chi_{\rm s}(\mathbf{r}_\parallel,0)\,],\ D/\mathcal{R}_x\to\infty\,, \tag{C.14}$$

which checks in three dimensions with the result (C.12).

Appendix D: The regime D, $\mathbf{R \ll \mathcal{R}_x}$

Consider a spherical particle near a wall (Fig. 1), with R and D much smaller than all the other mesoscopic lengths in the problem, for example $\mathcal{R}_x$ or the distance from the sphere to the fixed chain ends. The chains may be ideal or self-interacting. In the Ginzburg Landau description the exclusion of the integration region in (A.1) and the Dirichlet condition that arise from the presence of the spherical particle s can be represented in terms of the Boltzmann weight

$$\exp(-H_{\rm s}\{\boldsymbol{\Phi}\})\sim 1-R^d\,A_{\rm snw}(D/R)\,T_{\perp\perp}(\mathbf{0},0) \tag{D.1}$$

to leading order in small R and D. Here

$$T_{\perp\perp}(\mathbf{r}_\parallel,0)=\frac{1}{2}\left(\left[\partial_z\boldsymbol{\Phi}(\mathbf{r}_\parallel,z)\right]^2\right)_{z=0} \tag{D.2}$$

is the surface operator of the Dirichlet-wall with lowest scaling dimension that is even in $\boldsymbol{\Phi}$. It equals the component of the stress tensor at the surface of the wall perpendicular to the surface. Equation (D.1) is a generalization of equation (6.11) in reference [27], where the case $D=0$ is considered. It is similar to the short-distance expansion in field theories in unbounded space. The amplitude function $A_{\rm snw}$ is *independent* of the correlation function into which equation (D.1) is inserted and of t.

Equation (D.1) can be used to evaluate the free energy F for $R, D \ll \mathcal{R}_x$ since the integral in (3.2) is dominated by $|\mathbf{r}|$ of the order of $\mathcal{R}_x$. Note that [25]

$$\langle\mathcal{S}\cdot\varphi_{A,B}\rangle_{\rm h}=(\partial_{z_A}+\partial_{z_B})\langle\varphi_{A,B}\rangle_{\rm h}\,, \tag{D.3}$$

where

$$\mathcal{S}=\int \mathrm{d}\mathbf{r}_\parallel\,T_{\perp\perp}(\mathbf{r}_\parallel,0) \tag{D.4}$$

is the generator of a coordinate-shift (translation) away from the wall. From equations (A.4, D.1-D.4) and translational invariance of half space averages $\langle\,\rangle_{\rm h}$ parallel to the surface, the integral on the rhs of (3.2) tends to

$$\int_{\rm h}\mathrm{d}\mathbf{r}_A\,[\,\mathcal{E}_{\rm h}(z_A)-\mathcal{E}(\mathbf{r}_A)\,]\to R^d\,A_{\rm snw}\,\zeta_{\rm bulk}^{-1}\,\mathcal{L}\,I\,, \tag{D.5}$$

with

$$I=\int_0^\infty \mathrm{d}z_A\int_0^\infty \mathrm{d}z_B\,(\partial_{z_A}+\partial_{z_B})\,\chi_{\rm h}^{(l)}(z_A,z_B) \tag{D.6}$$

and the "*l*ayer-susceptibility"

$$\chi_{\rm h}^{(l)}(z_A,z_B)=\int \mathrm{d}\mathbf{r}_{B\parallel}\,\langle\varphi_{A,B}\rangle_{\rm h}\,. \tag{D.7}$$

Here $\mathbf{r}_{A\parallel}$, z_A denote components of $\mathbf{r}_A$ parallel and perpendicular to the wall, and a corresponding notation is used for $\mathbf{r}_B$. In equation (D.6) $\chi_{\rm h}^{(l)}$ can be replaced by $\chi_{\rm h}^{(l)}-\chi_{\rm bulk}^{(l)}$, where $\chi_{\rm bulk}^{(l)}(|z_A-z_B|)$ follows from $\langle\varphi_{A,B}\rangle_{\rm bulk}$ as $\chi_{\rm h}^{(l)}$ from $\langle\varphi_{A,B}\rangle_{\rm h}$ in equation (D.7). That $\chi_{\rm h}^{(l)}(z_B,0)$ vanishes implies

$$\begin{aligned} I&=2\int_0^\infty \mathrm{d}z_B\,\chi_{\rm bulk}^{(l)}(|z_B|)\\ &=\int \mathrm{d}\mathbf{r}_B\,\langle\varphi_{A,B}\rangle_{\rm bulk}\end{aligned} \tag{D.8}$$

and equations (3.2, D.5, D.8, A.5) lead to the result

$$Y_3(D/R)=A_{\rm snw}(D/R) \tag{D.9}$$

for the scaling function in (2.3).

The amplitude function $A_{\rm snw}$ in equation (D.1) may be determined from a calculation for $t=0$ and $|\mathbf{r}|\gg R, D$ of the average $\langle\boldsymbol{\Phi}^2(\mathbf{r})\rangle$ of the operator $\boldsymbol{\Phi}^2(\mathbf{r})$ in the "sphere in the half space" geometry of Figure 1. As discussed below, this leads to

$$A_{\rm snw}(\delta)=[\delta(\delta+2)]^{d/2}\,\tau(Q(\delta))\,C_T S_d/x_{\phi^2} \tag{D.10}$$

with $S_d=2\pi^{d/2}/\Gamma(d/2)$ the surface area of the d–dimensional unit sphere, $x_{\phi^2}=d-1/\nu$ the scaling dimension of $\boldsymbol{\Phi}^2$, C_T a universal amplitude in the short distance expansion [25,44]

$$\frac{\boldsymbol{\Phi}^2(\mathbf{r}_\parallel,z)}{\langle\boldsymbol{\Phi}^2(\mathbf{r})\rangle_{\rm h}}-1\to -C_T\,z^d\,T_{\perp\perp}(r_\parallel,0) \tag{D.11}$$

of $\boldsymbol{\Phi}^2$ about the Dirichlet wall, where $\langle\boldsymbol{\Phi}^2\rangle_{\rm h}$ is a $t=0$ profile, and with the universal function

$$\tau(Q)=-\hat{r}^d\,\langle T_{nn}(\hat{\mathbf{r}})\rangle_{\rm conc}\,. \tag{D.12}$$

Here $\langle\,\rangle_{\rm conc}$ denotes an average in a field theory at the critical point in the space bounded by two *concentric* spheres with radii R_- and R_+ where the fluctuating field $\boldsymbol{\Phi}$ vanishes, and T_{nn} is the radial component (normal to the spherical surfaces) of the stress tensor. The rhs of (D.12) is independent of the position $\hat{\mathbf{r}}$ between the concentric spheres ($\hat{r}$ denotes the distance from their midpoint) and depends only on the ratio $Q=R_-/R_+$, which is smaller than 1. Finally, the δ dependence of Q in (D.10) is given in equation (2.14b). For the case of ideal chains the field theory is Gaussian [21–23,26,27], and the explicit form of $\tau=\tau^{(\rm Gauss)}$ is given in equation (4.12) of reference [32]. Using $x_{\phi^2}^{(\rm Gauss)}=d-2$ and $C_T^{(\rm Gauss)}$ given in equation(4.24) of reference [32] (where it is denoted by $C_{\phi^2}^{(0)}$), one finds for $d=3$ the result for Y_3 given in equation (2.14).

Equation (D.10) also determines Y_3 for chains with excluded volume interactions once τ in (D.12) is known for the corresponding field theory of the n–vector model [21–23,26,27]. Here we only discuss two limits. In the limit $\delta \to 0$ where the sphere touches the wall

$$\tau(Q(\delta)) \to (1-d)\,\Delta\,(2\delta)^{-d/2}, \quad \delta \to 0\,, \tag{D.13}$$

where Δ is the universal Casimir amplitude in the term $k_{\rm B}T\Delta\mathcal{D}^{1-d}$ of the free energy per unit surface area in a field theory at the critical point in the space between two parallel planar surfaces with distance $\mathcal{D}$, as in equations (2.3, 2.4b) in [32]. In this limit $A_{\rm snw} = Y_3$ reduces to the expression for $A_{\rm ts}$ in equation (6.12) of reference [27]. In the opposite limit $D \gg R$ equation (D.10) leads to the behavior (2.5) of $A_{\rm snw} = Y_3$. This follows from

$$\tau(Q) \to S_d^{-1}\, x_{\phi^2}\, Q^{x_{\phi^2}}\, a, \quad Q \to 0\,, \tag{D.14}$$

as in equations(2.3, 2.13b) in reference [32] with a an universal amplitude defined in equations (A2, A3) of reference [27], when combined with the relation (6.7) in [27] between A, B and a, C_T.

To establish equation (D.10) we consider profiles of $\boldsymbol{\Phi}^2$ inside a spherical container of radius R_+, both in the presence ($\langle\boldsymbol{\Phi}^2\rangle_{\rm conc}$) and absence ($\langle\boldsymbol{\Phi}^2\rangle_{\rm fc}$) of a concentric spherical particle of radius R_-, and the relative deviation

$$\frac{\langle\boldsymbol{\Phi}^2(\hat{\mathbf{r}})\rangle_{\rm conc}}{\langle\boldsymbol{\Phi}^2(\hat{\mathbf{r}})\rangle_{\rm fc}} - 1 \to C_T \left(1 - \frac{\hat{r}}{R_+}\right)^d \tau(Q) \tag{D.15}$$

at the critical point as $\hat{r} \to R_+$ approaches the boundary of the container. Equation (D.15) follows from averaging (D.11) for a half space in the presence of a spherical particle (Fig. 1) and from a *conformal* transformation to the geometry of the spherical container [31,32], compare equations (2.18, 3.36) in reference [32], where $\mathbf{r}$ and $\hat{\mathbf{r}}$ are denoted by $\mathbf{r}'$ and $\mathbf{r}$, respectively. The relation (2.14b) between Q and δ expresses the conformal invariance of a cross-ratio. Of course, the $\hat{\mathbf{r}}$–dependence in (D.15) is spherically symmetric. Since the point $\hat{r} = R_+$ (on the boundary of the container) corresponds to $\mathbf{r} = \infty$ in the half space geometry, the leading behavior for $r \gg R, D$ can be obtained from (D.15) and is given by

$$\frac{\langle\boldsymbol{\Phi}^2(\mathbf{r})\rangle}{\langle\boldsymbol{\Phi}^2(\mathbf{r})\rangle_{\rm h}} - 1 \to R^d \left(\frac{2z}{r^2}\right)^d [\delta(\delta+2)]^{d/2}\, \tau(Q(\delta))\, C_T\,. \tag{D.16}$$

From this result (D.10) follows, since on using (D.1) the lhs of (D.16) is given by $R^d A_{\rm snw}\gamma(\mathbf{r})$, with the half-space quantity

$$\begin{aligned}\gamma(\mathbf{r}) &= -\langle T_{\perp\perp}(0)\cdot\boldsymbol{\Phi}^2(\mathbf{r})\rangle_{\rm h}/\langle\boldsymbol{\Phi}^2(\mathbf{r})\rangle_{\rm h} \\ &= \left(\frac{2z}{r^2}\right)^d x_{\phi^2}/S_d\,.\end{aligned} \tag{D.17}$$

For the last step see, *e.g.*, equation (2.13) in reference [44].

Appendix E: Force and stress tensor

With (A.4) for the end-density $\mathcal{E}$ one finds

$$F = p\,\zeta_{\rm bulk}^{-1}\,\mathcal{L}\int_{\rm h}\mathrm{d}\mathbf{r}_A\int_{\rm h}\mathrm{d}\mathbf{r}_B\,[\langle\varphi_{A,B}\rangle_{\rm h} - \langle\varphi_{A,B}\rangle] \tag{E.1}$$

for the free energy of interaction F in equation (3.2). The expression

$$\partial F/\partial D = p\,\zeta_{\rm bulk}^{-1}\,\mathcal{L}\int_{\rm h}\mathrm{d}\mathbf{r}_A\int_{\rm h}\mathrm{d}\mathbf{r}_B\,[\langle\mathcal{S}\cdot\varphi_{A,B}\rangle_{\rm h} - \langle\mathcal{S}\cdot\varphi_{A,B}\rangle] \tag{E.2}$$

for the force in terms of the shift-generator $\mathcal{S}$ in (D.4) follows from (E.1), equation (D.3) in the half-space without the particle and the corresponding relation,

$$\langle\mathcal{S}\cdot\varphi_{A,B}\rangle = (\partial_{z_A} + \partial_{z_B} + \partial_D)\langle\varphi_{A,B}\rangle\,, \tag{E.3}$$

in the presence of the particle. $\langle\varphi_{A,B}\rangle$ in equation (E1) and $\langle\mathcal{S}\cdot\varphi_{A,B}\rangle$ in equation (E2) are understood to vanish for $\mathbf{r}_A$ or $\mathbf{r}_B$ inside s. A more explicit form for the first quantity is $\Theta_{\rm h\backslash s}(\mathbf{r}_A)\Theta_{\rm h\backslash s}(\mathbf{r}_B)\langle\varphi_{A,B}\rangle$, with $\Theta_{\rm h\backslash s}$ projecting onto h\s (compare the caption of Figure 1). To obtain (E2) from (E1) and the shift identities, we have taken into account the following two facts: (i) $\partial_D(\Theta_{\rm h\backslash s}\Theta_{\rm h\backslash s}\langle\varphi_{A,B}\rangle)$ equals $\Theta_{\rm h\backslash s}\Theta_{\rm h\backslash s}\partial_D\langle\varphi_{A,B}\rangle$, since differentiating the characteristic functions (or, equivalently, the integration boundaries in $\int\mathrm{d}\mathbf{r}_A\int\mathrm{d}\mathbf{r}_B$) w.r.t. D does not contribute, because $\langle\varphi_{A,B}\rangle$ vanishes on the surface of h\s. (ii) The complete differential $(\partial_{z_A}+\partial_{z_B})[\langle\varphi_{A,B}\rangle_{\rm h} - \langle\varphi_{A,B}\rangle]$ does not contribute inside the integral $\int\mathrm{d}\mathbf{r}_A\int\mathrm{d}\mathbf{r}_B$, since the square bracket vanishes far away from s and on the surface of w and since $\langle\varphi_{A,B}\rangle$ vanishes on the surface of s.

Equations (E1, E2) apply both to ideal chains and chains with self-repulsion [29]. Below we concentrate on the former case, in which the cumulant averages in (E2) are Gaussian and *factor*, so that

$$\begin{aligned}\langle\mathcal{S}\cdot\varphi_{A,B}\rangle = &\int\mathrm{d}\mathbf{r}_\parallel\left(\partial_z\langle\Phi_1(\mathbf{r}_\parallel,z)\Phi_1(\mathbf{r}_A)\rangle\right)_{z=0} \\ &\times\left(\partial_z\langle\Phi_1(\mathbf{r}_\parallel,z)\Phi_1(\mathbf{r}_B)\rangle\right)_{z=0}\,,\end{aligned} \tag{E.4}$$

where equations (D.2, D.4) have been used. Since $\zeta_{\rm bulk} = 1$ and the susceptibility $\int\mathrm{d}\mathbf{r}_A\langle\Phi_1(\mathbf{r})\Phi_1(\mathbf{r}_A)\rangle$ equals the Laplace transform χ in equations (5.1, E.2, E.4) imply

$$\partial F/\partial D = p\mathcal{L}\int\mathrm{d}\mathbf{r}_\parallel\left[(\partial_z\chi_{\rm h}(\mathbf{r}))^2 - (\partial_z\chi(\mathbf{r}))^2\right]_{z=0}\,. \tag{E.5}$$

This leads to equation (5.12a), due to the defining equation (5.9) of $\mathcal{T}$ and the vanishing of χ on the surface $z = 0$ of the wall.

References

1. W.B. Russell, D.A. Saville, W.R. Schowalter, *Colloidal Dispersions* (Cambridge University, 1989).

2. *Colloid Physics*, proceedings of a workshop, Physica A **235**, 120 (1997).
3. P.R. Sperry, H.B. Hopfenberg, N.L. Thomas, J. Colloid Interface Sci. **82**, 62 (1980).
4. H. de Hek, A. Vrij, J. Colloid Interface Sci. **84**, 409 (1981).
5. A.P. Gast, W.B. Russell, C.K. Hall, J. Colloid Interface Sci. **109**, 161 (1986).
6. H.N.W. Lekkerkerker, Physica A**213**, 18 (1995).
7. W.C.K. Poon, S.M. Ilett, P.N. Pusey, Il Nuovo Cimento D **16**, 1127 (1994).
8. Y.N. Ohshima *et al.*, Phys. Rev. Lett. **78**, 3963 (1997).
9. D. Rudhardt, C. Bechinger, P. Leiderer, Phys. Rev. Lett. **81**, 1330 (1998).
10. R. Verma, J.C. Crocker, T.C. Lubensky, A.G. Yodh, Phys. Rev. Lett. **81**, 4004 (1998)
11. S. Asakura, F. Oosawa, J. Chem. Phys. **22**, 155 (1954); J. Polym. Sci. **33**, 183 (1958).
12. A. Yethiraj, C.K. Hall, R. Dickman, J. Colloid Interface Sci. **151**, 102 (1992).
13. P.G. Khalatur, L.V. Zherenkova, A.R. Khokhlov, Physica A **247**, 205 (1997).
14. A.P. Chatterjee, K.S. Schweizer, J. Chem. Phys. **109**, 10477 (1998)
15. E.J. Meijer, D. Frenkel, J. Chem. Phys. **100**, 6873 (1994).
16. E.M. Rozhkov, P.G. Khalatur, Colloid J. **58**, 778 (1996); P.G. Khalatur in *Methods in Contemporary Chemistry*, S.I. Kuchanov, edited by Gordon and Breach (New York, 1996).
17. P.G. de Gennes, C.R. Acad. Sc. Paris B **288**, 359 (1979).
18. E. Eisenriegler, A. Hanke, S. Dietrich, Phys. Rev. E **54**, 1134 (1996).
19. J.F. Joanny, L. Leibler, P.G. de Gennes, J. Polym. Sci., Polym. Phys. Ed. **17**, 1073 (1979).
20. T. Odijk, Macromolecules **29**, 1842 (1996); J. Chem. Phys. **106**, 3402 (1996).
21. P.G. de Gennes, *Scaling Concepts in Polymer Physics* (Cornell University, Ithaca, 1979).
22. J. des Cloizeaux, G. Jannink, *Polymers in Solution* (Clarendon, Oxford, 1990).
23. L. Schäfer, *Excluded Volume Effects in Polymer Solutions* (Springer, Heidelberg, 1999).
24. K. Binder, in *Phase Transitions and Critical Phenomena*, edited by C. Domb, J.L. Lebowitz (Academic Press, London, 1983), Vol. **8**.
25. (a) H.W. Diehl, in *Phase Transitions and Critical Phenomena*, edited by C. Domb, J.L. Lebowitz (Academic Press, London, 1986), Vol. **10**; (b) H.W. Diehl, International J. Mod. Physics B **11**, 3503 (1997).
26. E. Eisenriegler, *Polymers near Surfaces* (World Scientific, Singapore, 1993).
27. E. Eisenriegler, in *Field Theoretical Tools in Polymer - and Particle-Physics*, edited by H. Meyer-Ortmanns, A. Klümper, Lecture Notes in Physics **508** (Springer, Berlin, 1998).
28. B.V. Derjaguin, Kolloid Z. **69**, 155 (1934).
29. E. Eisenriegler, Phys. Rev. E **55**, 3116 (1997).
30. A. Hanke, E. Eisenriegler, S. Dietrich, Phys. Rev. E **59**, 6853 (1999).
31. T. Burkhardt, E. Eisenriegler, Phys. Rev. Lett. **74**, 3189 (1995).
32. E. Eisenriegler, U. Ritschel, Phys. Rev. B **51**, 13717 (1995).
33. A. Hanke, F. Schlesener, E. Eisenriegler, S. Dietrich, Phys. Rev. Lett. **81**, 1885 (1998).
34. For (2.8) compare Appendix B or equation (14) in reference [29], where $\mathcal{Y}(\vartheta,\infty)$ is denoted by $-V(\vartheta)$, and for (2.9) compare equation (2.2b) with $M_{\rm h}$ taken, *e.g.*, from equations (2.9, 2.11, 2.12) in E. Eisenriegler, J. Chem. Phys. **79**, 1052 (1983), where $M_{\rm h}$ is denoted by $\rho(z)/\rho_{\rm b}$.
35. See reference [27], where the strength of the *wall*-defect is calculated for $D = 0$, and where $A_{\rm snw}(0)$ and Y_3 are denoted by $A_{\rm ts}$ and J, respectively.
36. A. Milchev and K. Binder, Eur. Phys. J. B **3**, 477 (1998), have checked a corresponding density-force relation for a self avoiding polymer chain trapped between two parallel repulsive walls with Monte Carlo simulations.
37. M. Abramowitz, I.A. Stegun, *Handbook of Mathematical Functions* (Dover Publications, New York, 1972), see in particular pages 297, 437.
38. R. Lipowsky, Europhys. Lett. **30**, 197 (1995).
39. We first extend the **r**-integration in the representation of the weight function w over the *finite* part of h\s with $r < U$ and perform the limit $U \to \infty$ *after* the k-integration in (4.2) or (4.12).
40. $\mathcal{T}$ is the canonical stress tensor of the "Hamiltonian density" $\mathcal{K}$ in equation (5.4).
41. R.L. Burden and J.D. Faires, *Numerical Analysis* (PWS Publishing Company, Boston,1993).
42. F. Schlesener, Diploma thesis, University of Wuppertal (1997) (unpublished).
43. Y. Mao, M.E. Cates, H.N.W. Lekkerkerker, Physica A **222**, 10 (1995).
44. See E. Eisenriegler, M. Krech, S. Dietrich, Phys. Rev. B **53**,14377 (1996), and references cited therein.